

No.: egusphere-2024-2869

Title: Measurement report: Crustal materials play an increasing role in elevating particle pH: Insights from 12-year records in a typical inland city of China.

Reviewer #1:

General Comments:

In this article, the authors analyze 12 years of field observation data from Zhengzhou, China, to investigate trends in aerosol composition concentrations and its acidity. This approach is well-aligned with the scope and objectives of the “Measurement Report”, making the study highly relevant. However, there are contentious aspects in the discussion and final conclusions of this article. Specifically, whether crustal materials play a dominant role in driving the changes in aerosol acidity remains uncertain. This issue affects several parts of the article, including its main argument and even the title. I believe the authors are capable of making substantial revisions to the article.

Thank you for your careful reading of our paper and valuable comments and suggestions. We believe that we have adequately addressed your comments. To facilitate your review, we used yellow highlights for your comments, green highlights for Reviewer #2, and red color indicating our own corrections in the manuscript.

Major issues:

1. Lines 15-17: Compared to the reduction of ammonia emissions, the reductions in acidic precursors such as SO₂ and NO_x have been more significant, leading to an overall increase in atmospheric acidity (including aerosols, clouds, and precipitation). Studying the trends in aerosol acidity is highly meaningful, but it is essential to consider the combined impact of the reduction in both acidic and basic precursors.

Response: Thanks for your suggestion. This sentence has been modified to: “Particle acidity serves as a key determinant in atmospheric chemical processes. Emerging concerns regarding aerosol acidity trends have been highlighted amid China’s sustained initiatives to mitigate emissions of both acidic and alkaline precursors.”

2. Lines 19-21: The 12-year observation period and the corresponding years for the PM concentration results do not align. While I understand that the authors began observations in 2011, the abstract should be rephrased to ensure clarity and consistency in the presentation of the time frame.

Response: Sorry for the misunderstanding. This sentence has been modified to: “12-year observational data in Zhengzhou reveal that the annual average PM_{2.5} concentration decreased from $162 \pm 81 \mu\text{g}/\text{m}^3$ in 2011 to $60 \pm 41 \mu\text{g}/\text{m}^3$ in 2022, with the largest reduction in sulfate (73%). Correspondingly, the annual particle pH increased by 0.10 units from 2011 to 2019.”

3. Lines 28-29: According to mainstream forecasts regarding the need for further PM reduction under China's carbon peaking and carbon neutrality policy, future emission reduction strategies will primarily focus on acidic precursors. The expression here needs to be more precise and cautious.

Response: Thank you for your comment. This sentence has been modified to: "Therefore, the long-term evolution of particle acidity in North China will require comprehensive consideration of synergistic effects involving acidic precursors, ammonia, and crustal materials."

4. Lines 63-65: There is a lack of logical flow from the previous discussion of acidity changes to the conclusion/summary in this sentence. Additionally, aerosol acidity is unlikely to be neutral or even approach neutrality by nature in general.

Response: Sorry for the misunderstanding. This sentence has been modified to: "The atmospheric behavior of ammonium, governed by gas-particle partitioning processes involving ammonia (NH_3) as the predominant alkaline gas, demonstrates notable stability in concentration levels, with observational records showing less than 5% interannual variation in NH_3 column densities over North China during 2015–2019 (Dong et al., 2023). Under such conditions, the dominant inorganic aerosol component transitions from ammonium sulfate to ammonium nitrate. This compositional shift enhances atmospheric particulate hygroscopicity due to ammonium nitrate's superior

water uptake capability, ultimately elevating particle pH levels through aqueous-phase dilution mechanisms (Pinder et al., 2007, 2008; Heald et al., 2012; Weber et al., 2016).”

5. Lines 66-67: This may not be entirely accurate. The relative contribution of sulfate and nitrate does not directly determine aerosol acidity. The authors need to identify the true driving factors behind the pH trend. In my opinion, the main drivers are the $\text{NH}_3/\text{NH}_4^+$ multiphase buffering, ALWC, and non-volatile cations, rather than other components or temperature. This is because, over the long term, the impact of temperature variations on pH is minimal within the same season.

Response: Thank you for your comment. The observed transition in inorganic aerosol composition from ammonium sulfate to ammonium nitrate fundamentally alters aerosol hygroscopicity, as evidenced by deliquescence relative humidity differentials: NH_4NO_3 exhibits DRH = 61% versus 80% for $(\text{NH}_4)_2\text{SO}_4$ at 298K (ISORROPIA II model). This phase shift enhances water uptake by 38–72% (Wexler and Seinfeld, 1991). The consequent dilution effect on hydrogen ion concentration ($[\text{H}^+]$) leads to pH increases.

Therefore, this sentence has been modified to: “This compositional shift enhances atmospheric particulate hygroscopicity due to ammonium nitrate’s superior water uptake capability, ultimately elevating particle pH levels through aqueous-phase dilution mechanisms (Wexler and Seinfeld, 1991; Pinder et al., 2007, 2008; Heald et al., 2012; Weber et al., 2016). For instance, a significant increase in the nitrate-to-sulfate molar ratio from 2014–2017 in Beijing resulted in the particle pH increasing from 4.4

to 5.4 (Xie et al., 2020).”

6. Lines 85-86: Given the limitations, under what circumstances does it go from 4 to 7?.

Response: Thank you for your careful reading of our paper. This sentence has been modified to: “Karydis et al. (2021) framework demonstrated that CM played a critical buffering role in sustaining aerosol pH around 7 across the Middle East arid regions. The model sensitivity tests revealed that under hypothetical dust-free conditions (CM = 0), aerosol acidity would escalate to pH~4 due to $\text{NH}_4^+/\text{SO}_4^{2-}$ domination.”

7. Lines 93-94: After reviewing the research progress, I suggest concluding with a summary that introduces the focus of this article. Specifically, what makes Zhengzhou and other cities different, what issue this study aims to address based on previous research, and what contributions this study makes. This is essential in scientific writing.

Response: Thank you for your comment. We have added a description in revised version:

“Zhengzhou presents unique atmospheric chemistry that distinguishes it from other mega-cities in North China. As the capital of China’s foremost agricultural province (Henan Province, contributing 18% of national NH_3 emissions), Zhengzhou’s $\text{PM}_{2.5}$ composition combined substantial crustal material ($15 \pm 3\%$ in $\text{PM}_{2.5}$ vs. $<10\%$ in Beijing) with exceptional ammonia abundance (Huang et al., 2012; Liu et al., 2018;

Wang et al., 2018). This created distinct particle acidity characteristics, maintaining pH 4.5–6.0 compared to lower pH levels (3.3–5.4) in other cities like Beijing (Ding et al., 2019; Zhang et al., 2021). However, two critical research gaps persist: (1) the long-term evolution of CM under control policies remains unquantified; (2) the role of CM on pH buffer capacity in NH₃-enriched environments lacks systematic assessment.

To address these gaps, our study pioneers the first multi-decadal analysis (2011–2022) coupling PM_{2.5} components with thermodynamic modeling through three key innovations: (1) revealing the long-term trends of CM, (2) analyzing the variations of CM sources, and (3) exploring pH trend and its relationship with CM. The resultant findings advance our understanding of urban aerosol acidity chemistry by underscoring the critical role of CM.”

8. Line 123: Provide the version of ISORROPIA and the time resolution of the input components.

Response: Thank you for your suggestion. This sentence has been modified to: “The particle pH was calculated using the ISORROPIA-II mode (version 2.1, <http://isorropia.eas.gatech.edu>). The input data (excluding $RH \leq 30\%$), including SO_4^{2-} , TNO_3 ($HNO_3 + NO_3^-$), TNH_x ($NH_3 + NH_4^+$), Ca^{2+} , K^+ , Na^+ , Mg^{2+} , Cl^- , RH and T, with the temporal resolution aligned with the sampling periods (from 10:00 AM to 9:00 AM the following day).”

9. Line 160: The spring of 2021 saw multiple rare dust storms in the North China Plain, but why was the CM not high in 2021? Additionally, the resolution of the figures in both the main text and SI needs to be improved to at least 300 dpi, as many figures in the SI are unclear.

Response: Thank you for your comments.

“The quality assurance protocol excluded temporally discrete dust storm and precipitation periods to prevent contamination of the source analysis of CM and modeling particle pH, given that such events induce non-representative extremes in both crustal element concentrations and pH values, coupled with elevated PM measurement uncertainties.” In the revised manuscript, this quality control protocol description has been incorporated into Section 2.1 of the Methodology chapter.

Additionally, the resolution of the figures in both the main text and SI has been adjusted to 600 dpi.

10. Line 170 (Figure S3): It is recommended to use the same y-axis range for consistency. Regarding the drivers of seasonal variations (increase or decrease), I believe the discussion here lacks sufficient rigor, with an incomplete chain of evidence. I suggest that the authors consider separately discussing natural and anthropogenic sources, especially the impact of spring dust storm events on dust levels. In section 3.3, the source-related discussion is also mentioned, and therefore, this part needs to be strengthened.

Response: Thank you for your comments. We have replotted the Figure S5.

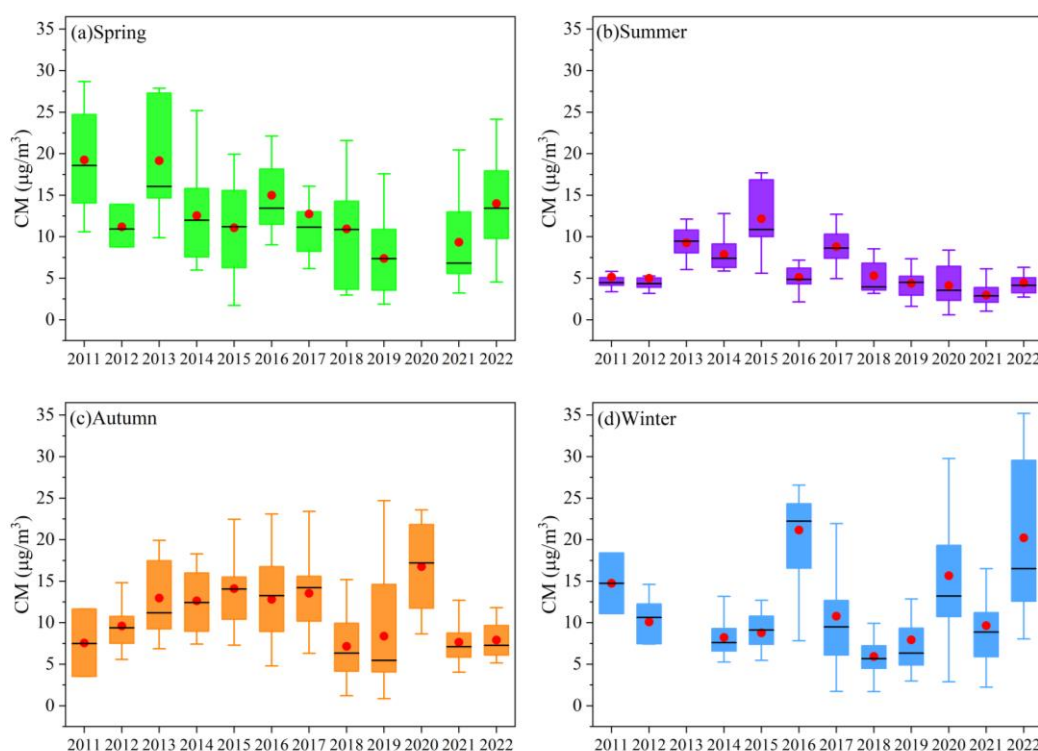


Figure S5. Trends in the CM concentrations in different seasons from 2011 to 2022.

We agree with your comment that the explanation of the seasonal variation characteristics lacked precise evidence. Therefore, we have revised the descriptions for different seasons and added figures showing the trends of wind speed (WS) and relative humidity (RH) changes across different seasons. However, as mentioned earlier, the data for dust storm events have been removed, and therefore, we cannot distinguish between natural and anthropogenic sources of dust. The revised description is as follows:

“Seasonal trends (Fig. S5) reveal significant declines in CM during spring in 2013–2019 with WS decreasing from 2.2 m/s in 2013 to 1.4 m/s in 2019 (Fig. S6) and stable RH (Fig. S7). Similarly, summer CM reductions in 2013–2019 corresponded

with WS declines. These patterns suggest spring-summer CM improvements resulted from the synergistic effects of meteorological changes and dust control policies. Conversely, autumn-winter seasons showed limited CM reductions despite comparable WS decreases in 2013–2019, highlighting the need for enhanced dust emission controls in Zhengzhou during these seasons.”

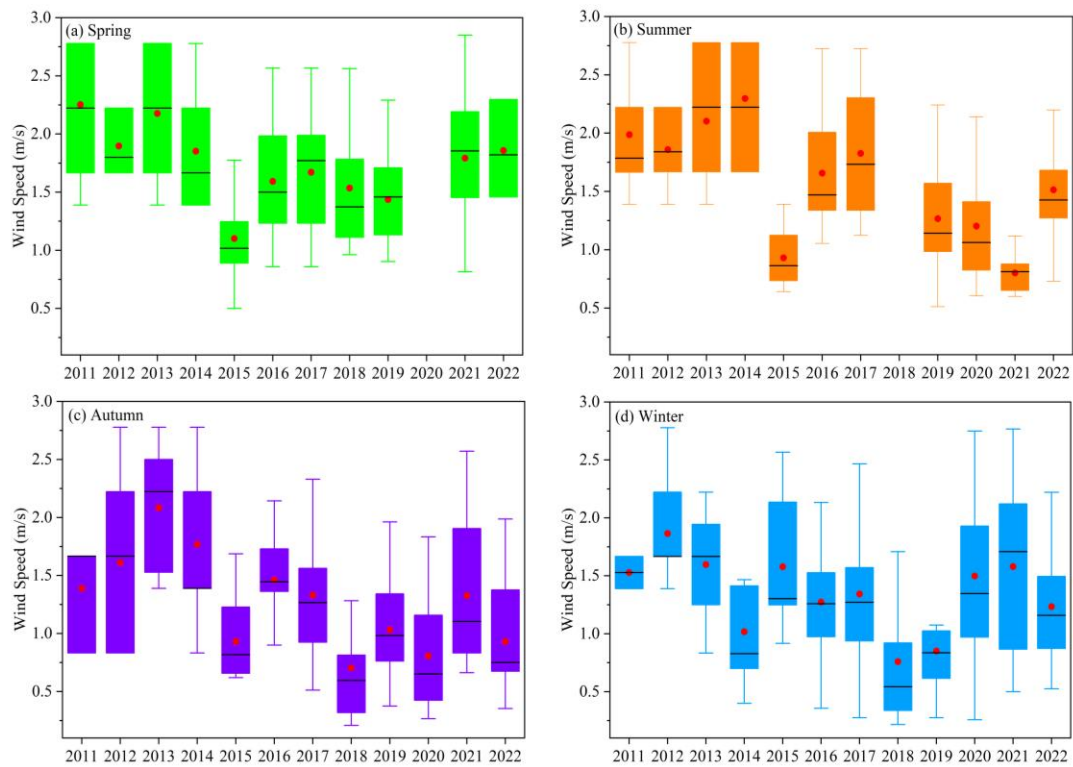


Figure S6 The variation in WS across different seasons from 2011 to 2022.

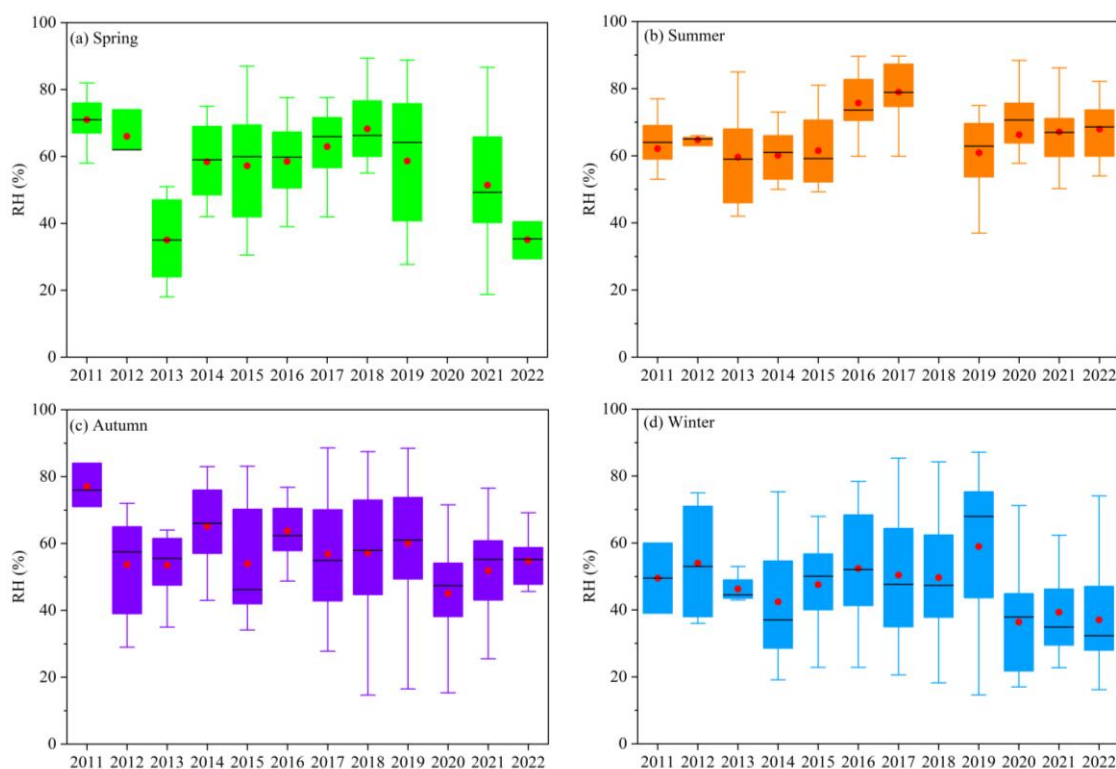


Figure S7 The variation in RH across different seasons from 2011 to 2022.

11. Lines 239-241: I believe ALWC is an important factor influencing pH, and it should not be solely attributed to sulfate. The authors need to carefully consider this point. Specifically, it should be evaluated whether the continuous decrease in ALWC affects pH, and whether this impact might even outweigh the influence of changes in aerosol composition.

Response: Thank you for your comments. We added the description on ALWC:

“According to Equation (2), in addition to H^+ concentration, particle pH is primarily influenced by the dilution effect of ALWC. Moreover, ALWC affects the gas-particle partitioning of semi-volatile compounds, thereby influencing particle acidity (Zuend et al., 2010; Zuend and Seinfeld, 2012). As shown in Fig.5 and Table S6, only

in 2015, 2019, and 2020 did the increases in ALWC concentration ($17.6 \mu\text{g}/\text{m}^3$, $4.1 \mu\text{g}/\text{m}^3$, and $11.6 \mu\text{g}/\text{m}^3$, respectively) lead to pH increases of 0.22, 0.06, and 0.14 units. This clearly cannot fully explain the significant pH increase in Zhengzhou since 2013. Notably, since 2013, H^+ concentration has shown a decreasing trend. Particularly, H^+ concentrations decreased by 7.6×10^{-6} , 11.2×10^{-6} , and $7.2 \times 10^{-6} \text{ mol/L}$ in 2013, 2015, and 2017, respectively, leading to pH increases of 0.21, 0.36, and 0.42 units. After 2019, a continuous decline in H^+ concentration was observed for three consecutive years, resulting in pH increases of 0.21, 0.13, and 0.2 units in 2020, 2021, and 2022, respectively. These findings indicate that the increase in pH from 2019 to 2022 in Zhengzhou was primarily driven by the reduction in H^+ concentration.

The concentration of H^+ in the aerosol liquid phase is influenced by both chemical composition and meteorological conditions. To further understand the factors affecting ΔpH , we analyzed the variations in $\text{PM}_{2.5}$ chemical components and meteorological parameters. Results indicate that the decline in SO_4^{2-} from 2013 to 2018 was the primary cause of the increase in particle pH, as it decreased H^+ and ALWC concentrations (Fig. S11) in aerosol (Ding et al., 2019; Zhang et al., 2021).”

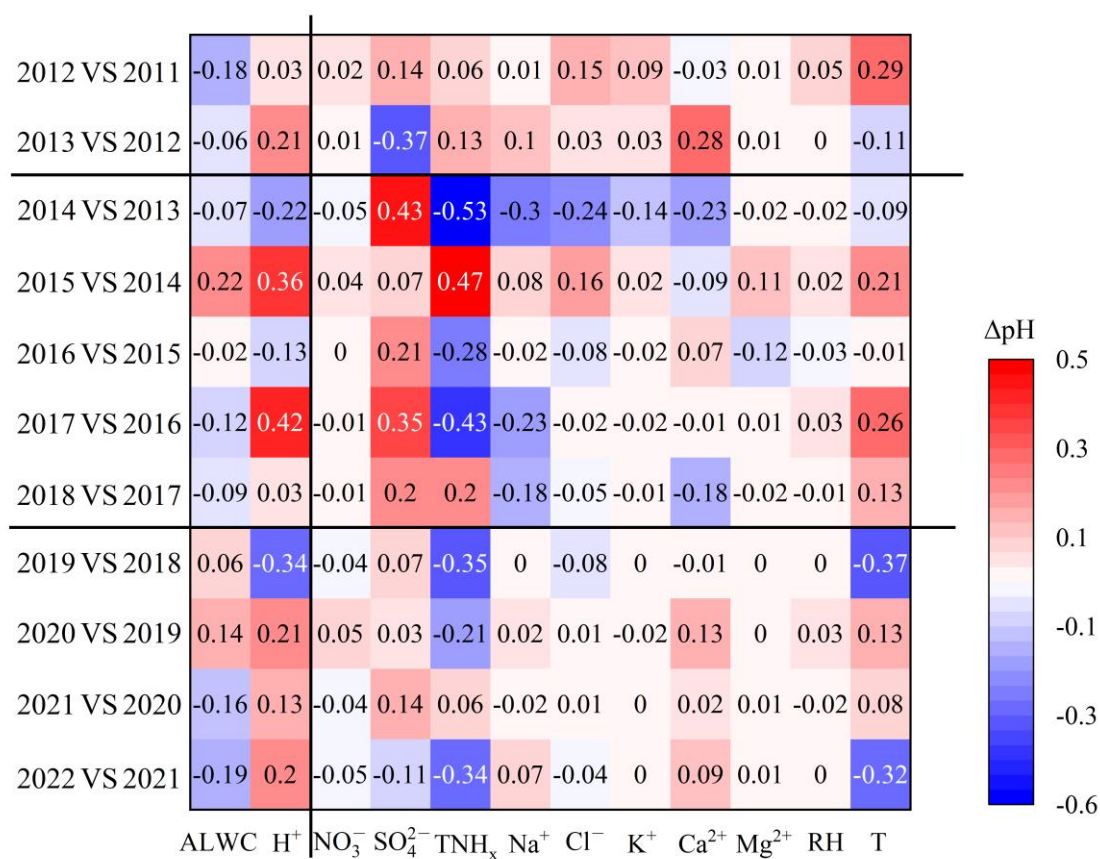


Figure 1. Contribution of each component to the changes in pH (ΔpH) between adjacent years. The difference between ALWC, H⁺, particle component concentrations, and meteorological parameters between adjacent years is listed in Table S6.

Table S6. The difference between component concentrations ($\mu\text{g}/\text{m}^3$) and meteorological parameters between adjacent years.

Years	ALWC	$\text{H}^+(\text{10}^{-6})$	NO_3^-	SO_4^{2-}	TNH_x	Na^+	Cl^-	K^+	Ca^{2+}	Mg^{2+}	RH(%)	T ($^{\circ}\text{C}$)
2012VS2011	-19.0	-1.5	4.0	-4.6	1.3	0.02	2.0	0.9	-0.2	0.04	-9.6	-5.7
2013VS2012	-4.6	-7.6	2.6	13.0	2.1	0.2	0.4	0.3	1.4	0.1	-2.6	2.1
2014VS2013	-4.5	7.9	-7.3	-14.6	-6.9	-0.4	-3.4	-1.6	-1.1	-0.2	6.6	2.0
2015VS2014	17.6	-11.2	5.2	-1.8	5.5	0.1	2.1	0.4	-0.6	0.6	-5.6	-4.2
2016VS2015	-2.3	3.0	-0.2	-4.5	-3.7	-0.03	-0.1	-0.4	0.5	-0.7	8.0	0.3
2017VS2016	-10.0	-7.2	-2.9	-5.3	-3.6	-0.2	-0.3	-0.2	-0.1	0.1	-6.0	-4.9
2018VS2017	-5.8	-0.3	-0.8	-2.4	1.3	-0.1	-0.8	-0.2	-0.1	-0.1	1.4	-2.8
2019VS2018	4.1	4.8	-3.0	-0.8	-2.2	-0.04	-0.7	-0.03	-0.1	-0.01	-0.1	7.3
2020VS2019	11.6	-3.4	4.9	-0.3	-0.9	0.1	0.1	-0.2	0.7	0.02	-6.6	-2.1
2021VS2020	-12.7	-1.5	-3.6	-2.3	0.2	-0.01	0.03	0.01	0.1	0.04	-2.8	-1.5
2022VS2021	-10.6	-1.5	-5.1	1.9	-1.4	0.03	-0.3	0.01	0.5	0.04	4.7	5.8

12. Lines 280-282: Where is the data for this section sourced from?

Response: This dataset was obtained from the China National Environmental Monitoring Center (CNEMC) and has been referenced in Section 2.1:

“The annual mean PM_{2.5} concentration data for cities in the North China Plain were obtained from the China National Environmental Monitoring Center (CNEMC), available at <https://www.cnemc.cn/>.”

13. Lines 283-286: Although many researchers have done significant work on the impact of ammonia reduction on PM levels, I believe that under China’s current policies, future emission reductions will not primarily focus on ammonia. Therefore, the authors need to reconsider whether the focus of this "Measurement Report" should be placed on ammonia. I suggest that the authors revise all statements related to ammonia, including the title.

Response: We sincerely thank the reviewer for their thoughtful and constructive feedback. Your point about the non-primary focus on ammonia reduction under current Chinese policies is well taken, and the sentence has been modified to: “Thus, crustal materials persist as a substantial constituent of atmospheric aerosols in North China, sustaining elevated particle pH levels. Extensive research has established that heightened particle pH inhibits nitrate reduction in aerosols (Ding et al., 2019; Lin et al., 2020; Wen et al., 2018), particularly significant given nitrate’s predominant role in

haze formation within this region. Notably, while moderately acidic aerosols demonstrate reduced health impacts, particles with $\text{pH} < 3$ exhibit substantially greater health risks (Shi et al., 2019). Consequently, future environmental management strategies must prioritize real-time assessment of regulatory impacts on particle acidity. This necessitates an integrated approach that simultaneously addresses acidic precursors, alkaline precursors, and crustal material contributions to atmospheric acid chemistry.

1 **Manuscript**

2 **Measurement report: Crustal materials play an increasing role**
3 **in elevating particle pH: Insights from 12-year records in a**
4 **typical inland city of China.**

5 Hongyu Zhang^{1,2}, Shenbo Wang^{2,3*}, Zhangsen Dong^{1,2*}, Xiao Li^{2,3}, Ruiqin Zhang^{2,3}

6

7 ¹ Collage of Chemistry, Zhengzhou University, Zhengzhou, 450000, China

8 ² Research Institute of Environmental Sciences, Zhengzhou University, Zhengzhou
9 450000, China

10 ³ School of Ecology and Environment, Zhengzhou University, Zhengzhou, 450000,
11 China

12

13 * Corresponding authors: Shenbo Wang and Zhangsen Dong

14 E-mail address: shbwang@zzu.edu.cn and dzszzu1990@163.com

15

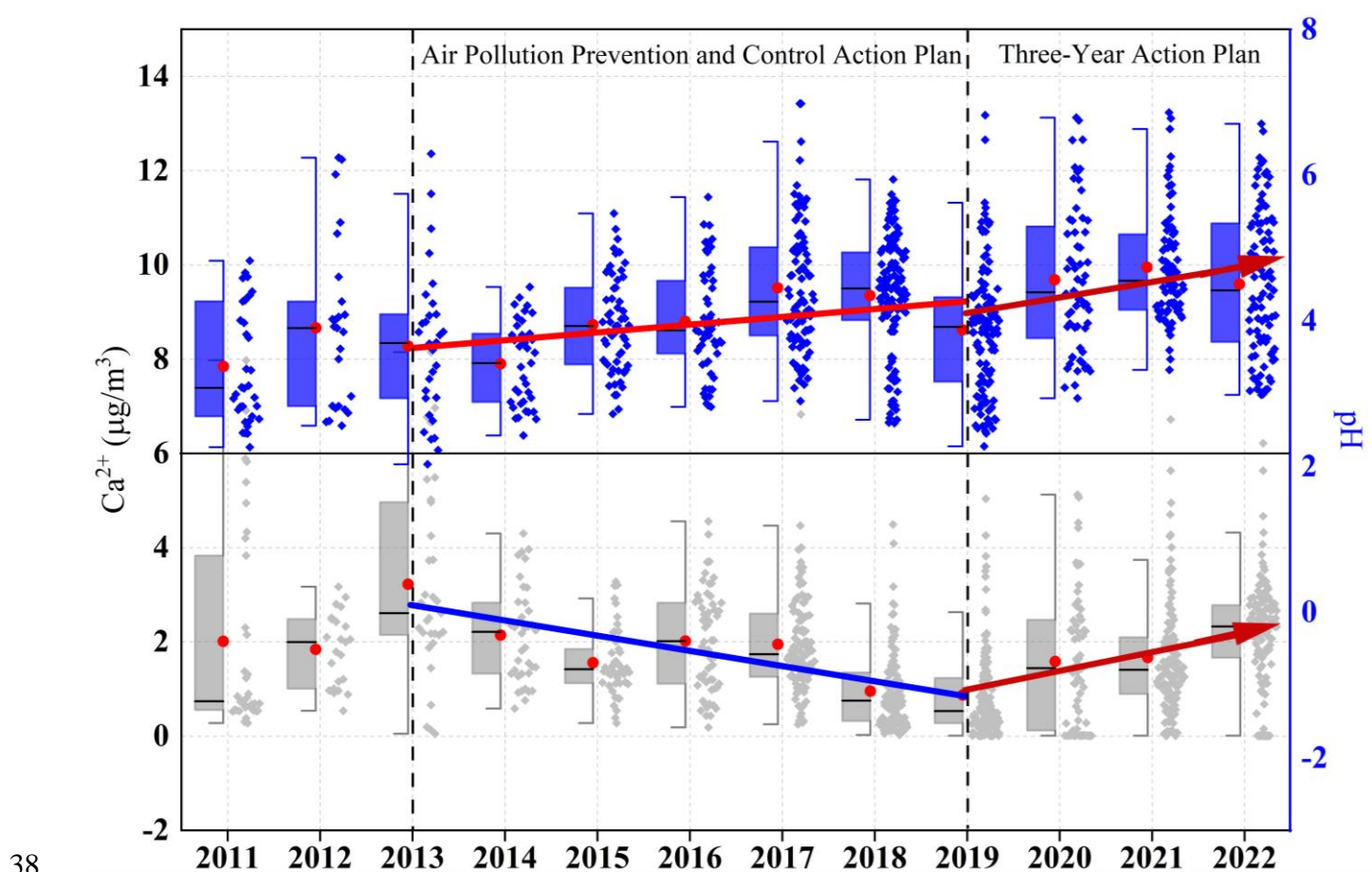
Abstract

Particle acidity serves as a key determinant in atmospheric chemical processes. Emerging concerns regarding aerosol acidity trends have been highlighted amid China's sustained initiatives to mitigate emissions of both acidic and alkaline precursors, especially in North China, which is significantly affected by dust aerosol. 12-year observational data in Zhengzhou reveal that the annual average $\text{PM}_{2.5}$ concentration decreased from $162 \pm 81 \mu\text{g}/\text{m}^3$ in 2011 to $60 \pm 41 \mu\text{g}/\text{m}^3$ in 2022, with the largest reduction in sulfate (73%). Correspondingly, the annual particle pH increased by 0.10 units from 2011 to 2019. In addition, the elevated particle pH in 2015 and 2018 was notably influenced by the increase in TNH_x ($\text{NH}_3 + \text{NH}_4^+$). Note that the crustal material concentrations and their proportions increased significantly during 2019–2022, which might be responsible for the resuspension of surrounding soil dust. Even though the TNH_x concentration was decreasing, the annual average growth rate of pH values increased to 0.21 units from 2019 to 2022. This phenomenon is not unique to Zhengzhou, as major cities in the North China Plain have also experienced a pronounced upward trend in coarse particles after 2019. Therefore, the long-term evolution of particle acidity in North China will require comprehensive consideration of synergistic effects involving acidic precursors, ammonia, and crustal materials.

Keywords: Dust, aerosol acidity, sources, North China Plain, control measurement

Synopsis: The future ammonia reduction policies in North China may not lead to a rapid increase in particle acidity in the presence of crustal materials., which further elevated the particle pH after 2019.

37 Graphical abstract:



39 Highlights:

- 40 • Crustal material concentrations and their proportions increased significantly during 2019–2022;
- 41 • The resuspension of surrounding soil dust may determine the rebound of crustal material
- 42 concentrations;
- 43 • Rebound in crustal material further elevated the particle pH.

44 1 Introduction

45 Particle acidity is a critical parameter that affects atmospheric chemistry, such as the gas-particle

46 partitioning of semi-volatile and volatile species (Surratt et al., 2010; Guo et al., 2016), the solubility
47 of metals (Tao and Murphy, 2019), acid-catalyzed reactions (Rengarajan et al., 2011), and acid
48 deposition (Mao et al., 2009), thereby determining aerosol concentration and chemical composition,
49 as well as impacting human health, ecosystems, and climate (Li et al., 2017; Pye et al., 2020; Su et al.,
50 2020; Nenes et al., 2021). Generally, the global fine particulate matter ($\text{PM}_{2.5}$, aerodynamic diameter
51 $\leq 2.5 \mu\text{m}$) exhibits a bimodal pH distribution ranging from 1–3 (e.g., in the United States and Europe)
52 (Guo et al., 2015; Battaglia et al., 2017; Masiol et al., 2020; Zhang et al., 2021) and 4–5 (e.g., in East
53 Asia) (Kim et al., 2022; Sharma et al., 2022). The atmosphere rich in gaseous ammonia (NH_3) and
54 crustal material (CM) shows significant pH buffering effects (Wang et al., 2020; Zheng et al., 2020;
55 Karydis et al., 2021), which is a dominant factor that drives the high particle pH in East Asia (Karydis
56 et al., 2021; Zhang et al., 2021; Kim et al., 2022; Sharma et al., 2022).

57 In recent years, the changing trends in particle pH have become a research focus, especially in
58 China, in response to air pollution control policies, i.e. Air Pollution Prevention and Control Action
59 Plan (2013–2018) and Three-Year Action Plan (2018–2020). The annual average $\text{PM}_{2.5}$ concentration
60 in Beijing dropped by 64% from $89.5 \mu\text{g}/\text{m}^3$ in 2013 to $32 \mu\text{g}/\text{m}^3$ in 2023 (MEP, 2023), with a clear
61 downward trend of sulfate concentration, and nitrate surpassing sulfate as the primary component (Zhai
62 et al., 2019; Zhou et al., 2019; Li et al., 2023). The atmospheric behavior of ammonium, governed by
63 gas-particle partitioning processes involving ammonia (NH_3) as the predominant alkaline gas,
64 demonstrates notable stability in concentration levels, with observational records showing less than 5%
65 interannual variation in NH_3 column densities over North China during 2015–2019 (Dong et al., 2023).
66 Under such conditions, the dominant inorganic aerosol component transitions from ammonium sulfate

67 to ammonium nitrate. This compositional shift enhances atmospheric particulate hygroscopicity due
68 to ammonium nitrate's superior water uptake capability, ultimately elevating particle pH levels through
69 aqueous-phase dilution mechanisms (Wexler and Seinfeld, 1991; Pinder et al., 2007, 2008; Heald et
70 al., 2012; Weber et al., 2016). For instance, a significant increase in the nitrate-to-sulfate molar ratio
71 from 2014–2017 in Beijing resulted in the particle pH increasing from 4.4 to 5.4 (Xie et al., 2020).
72 Moreover, increased NH_3 concentrations raised particle pH by 0.3–0.4 units from 2014/2015 to
73 2018/2019 in Beijing (Song et al., 2019). Over Europe and North America, the pH has increased
74 strongly from about 2.8 and 2.2 during the 1970s to 3.9 and 3.3 in 2020 respectively, especially during
75 the 1990s, with significantly increasing NH_3 emission (Karydis et al., 2021). On the contrary, modeling
76 results indicate a continuous decline in pH in East Asia from 1970 to 2020 due to sharp increases in
77 SO_2 and NO_x emissions (Karydis et al., 2021). In addition, the $\text{PM}_{2.5}$ pH showed a slight decrease of
78 0.13 from 2018 to 2022 summer in Beijing due to the change in total nitrate ($\text{NO}_3^- + \text{HNO}_3$) (Li et al.,
79 2023). Moreover, Zhou et al. (2022) found a decreasing pH trend from 2011 to 2019 in eastern China,
80 primarily influenced by temperature, followed by sulfate and non-volatile cations. Similarly, Nah et al.
81 (2023) observed a decreasing pH trend from 2011 to 2020 in Hong Kong, attributing it to temperature
82 and sulfate levels. Thus, concerns have been raised about the potential increase in the acidity of aerosol
83 and precipitation due to China's ongoing efforts to reduce ammonia emissions, which pose severe
84 health risks and acid deposition (Liu et al., 2019; Shi et al., 2019).

85 In addition to NH_3 , CM is another key alkaline substance, that buffers particle pH. Ca^{2+} can form
86 insoluble CaSO_4 with sulfate, reducing sulfate concentration in the aqueous phase of aerosol, and thus
87 lowering H^+ and aerosol liquid water content (ALWC) concentrations and enhancing particle pH (Ding

et al., 2019; Karydis et al., 2021). Moreover, non-volatile cations can lower the molar ratio of ammonia to sulfate, leading to an increase in particle pH (Zheng et al., 2022). Karydis et al. (2021) framework demonstrated that CM played a critical buffering role in sustaining aerosol pH around 7 across the Middle East arid regions. The model sensitivity tests revealed that under hypothetical dust-free conditions ($CM = 0$), aerosol acidity would escalate to $pH \sim 4$ due to NH_4^+/SO_4^{2-} domination. Wang et al. (2022) reported that non-volatile cations accounted for approximately 8–17% of hourly aerosol pH variation. Li et al. (2023) indicated that the buffering effect of cations was the major reason for the relatively small pH changes from 2018 to 2022 in Beijing, emphasizing that reducing coarse particle emissions in the future could significantly decrease particle pH. In addition, there was a rising trend in the contribution of CM to particle pH in Tianjin, China (Shi et al., 2017). Therefore, it is evident that CM has a significant impact on the variation of particle pH, especially in North China, which is significantly affected by dust aerosol, but the trend of CM concentration and its long-term implication is still lacking unfortunately.

Zhengzhou presents unique atmospheric chemistry that distinguishes it from other mega-cities in North China. As the capital of China's foremost agricultural province (Henan Province, contributing 18% of national NH_3 emissions), Zhengzhou's $PM_{2.5}$ composition combined substantial crustal material ($15 \pm 3\%$ in $PM_{2.5}$ vs. $<10\%$ in Beijing) with exceptional ammonia abundance (Huang et al., 2012; Liu et al., 2018; Wang et al., 2018). This created distinct particle acidity characteristics, maintaining pH 4.5–6.0 compared to lower pH levels (3.3–5.4) in other cities like Beijing (Ding et al., 2019; Zhang et al., 2021). However, two critical research gaps persist: (1) the long-term evolution of CM under control policies remains unquantified; (2) the role of CM on pH buffer capacity in NH_3 -

109 enriched environments lacks systematic assessment.

110 To address these gaps, our study pioneers the first multi-decadal analysis (2011–2022) coupling
111 PM_{2.5} components with thermodynamic modeling through three key innovations: (1) revealing the
112 long-term trends of CM, (2) analyzing the variations of CM sources, and (3) exploring pH trend and
113 its relationship with CM. The resultant findings advance our understanding of urban aerosol acidity
114 chemistry by underscoring the critical role of CM.

115 2 Experiment and method

116 2.1 Instruments and Measurements

117 Sampling was conducted on the fourth-floor platform at Zhengzhou University (34.75° N, 113.61°
118 E) in Zhengzhou, China. The sampling site (Fig. S1), approximately 14 m above the ground, is
119 primarily surrounded by residential areas with well-developed transportation networks and no
120 significant industrial sources. There are two highways located 3 km to the south and 7 km to the east.
121 Additionally, a coal-fired power plant located 6 km to the east was shut down in 2020, and a gas-fired
122 power plant is situated 3 km to the south.

123 Samples were collected using a high-volume sampler (TE-6070D, Tisch, USA) and air particulate
124 samplers (TH-16A, Tianhong, China) from April 2011 to December 2022. Two quartz filters and two
125 Teflon filters were used daily from 10:00 AM to 9:00 AM the next day, resulting in a total of 5848
126 samples. After excluding abnormal data due to instrument malfunctions, 4228 valid samples were
127 obtained. Detailed information on the samples is provided in Table S1. Organic carbon (OC) and
128 elemental carbon (EC) were analyzed using a carbon analyzer (Model 5L, Sunset Laboratory, USA).

Water-soluble inorganic ions (Cl^- , NO_3^- , SO_4^{2-} , Na^+ , NH_4^+ , K^+ , Mg^{2+} , and Ca^{2+}) were measured using ion chromatography (ICS-90 and ICS-900 models, Dionex, USA) (Yu et al., 2017; Jiang et al., 2018). Elements were analyzed using a wavelength dispersive X-ray fluorescence spectrometer (S8 TIGER, Bruker, Germany) to determine concentrations of Fe, Na, Mg, Al, Si, Cl, K, Ca, V, Ni, Cu, Zn, Cr, Mn, Co, Cd, Ga, As, Se, Sr, Sn, Sb, Ba, and Pb (Tremper et al., 2018). Meteorological conditions, including temperature (T), relative humidity (RH), and wind speed (WS) were obtained using an automatic weather station (Wang et al., 2019). Blank filters were also routinely analyzed with each batch of samples to detect sample contamination and provide quality assurance on the elemental concentrations. Detailed analytical methods and quality control are described in the supplement (Text S1). The method detection limits and measurement uncertainties are summarized in Table S2. The quality assurance protocol excluded temporally discrete dust storm and precipitation periods to prevent contamination of the source analysis of CM and modeling particle pH, given that such events induce non-representative extremes in both crustal element concentrations and pH values, coupled with elevated PM measurement uncertainties. The annual mean $\text{PM}_{2.5}$ concentration data for cities in the North China Plain were obtained from the China National Environmental Monitoring Center (CNEMC), available at <https://www.cnemc.cn/>.

2.2 Data Analysis

2.2.1 Mass reconstruction

The calculation method for CM is as follows (Tian et al., 2016):

$$[\text{CM}] = 1.89 \times [\text{Al}] + 2.14 \times [\text{Si}] + 1.4 \times [\text{Ca}] + 1.43 \times [\text{Fe}] + 1.94 [\text{Ti}] \quad (1)$$

149 where [Al], [Si], [Ca], [Fe] and [Ti] represent the concentrations of the respective elements ($\mu\text{g}/\text{m}^3$),
 150 but Ti was not measured.

151 2.2.2 Thermodynamic model

152 The particle pH was calculated using the ISORROPIA-II mode (version 2.1,
 153 <http://isorrophia.eas.gatech.edu>). The input data (excluding $\text{RH} \leq 30\%$), including SO_4^{2-} , TNO_3 (HNO_3
 154 $+\text{NO}_3^-$), TNH_x ($\text{NH}_3+\text{NH}_4^+$), Ca^{2+} , K^+ , Na^+ , Mg^{2+} , Cl^- , RH and T, with the temporal resolution aligned
 155 with the sampling periods (from 10:00 AM to 9:00 AM the following day). Input data (excluding RH
 156 $\leq 30\%$) included SO_4^{2-} , TNO_3 ($\text{HNO}_3 + \text{NO}_3^-$), TNH_x ($\text{NH}_3+\text{NH}_4^+$), Ca^{2+} , K^+ , Na^+ , Mg^{2+} , Cl^- , RH and
 157 T. The concentrations of hydrogen ions in air (H_{air}^+) and ALWC were calculated using the aerosol
 158 equilibrium composition system $\text{Na}^+ - \text{K}^+ - \text{Ca}^{2+} - \text{Mg}^{2+} - \text{NH}_4^+ - \text{SO}_4^{2-} - \text{NO}_3^- - \text{Cl}^- - \text{H}_2\text{O}$ H_{air}^+ (Fountoukis and
 159 Nenes, 2007). pH values were calculated using the following formula:

$$160 \quad \text{pH} = -\log_{10} \text{H}_{\text{aq}}^+ \cong -\log_{10} \frac{1000 \text{H}_{\text{air}}^+}{\text{ALWC}_i + \text{ALWC}_o} \cong -\log_{10} \frac{1000 \text{H}_{\text{air}}^+}{\text{ALWC}_i} \quad (2)$$

$$161 \quad \text{ALWC}_o = \frac{m_{\text{org}} \rho_w}{\rho_w} \frac{K_{\text{org}}}{\left(\frac{1}{\text{RH}} - 1 \right)} \quad (3)$$

162 where ALWC_i and ALWC_o refer to the ALWC for inorganic and organic components, respectively.
 163 m_{org} denotes the mass of organic aerosol, ρ_w is the density of water ($1.0 \text{ g}/\text{cm}^3$), ρ_{org} is the density of
 164 organic material ($1.4 \text{ g}/\text{cm}^3$) (Guo et al., 2015), K_{org} is the hygroscopicity parameter for organic aerosol
 165 (0.087) (Chang et al., 2010; Li et al., 2016). The ISORROPIA-II model operated under metastable
 166 conditions in the forward mode. Due to the lack of measured data for gaseous HNO_3 and NH_3 , TNO_3
 167 was represented solely by NO_3^- . The concentration of NH_3 was simulated based on a linear regression

equation proposed by Wei et al. (2023), who used the same data as this study from 2013 to 2020:

$$\text{NH}_3 = 19.909 \times \text{RH} + 0.559 \times \text{T} - 0.35 \times \text{NH}_4^+ + 0.123 \times \text{NO}_3^- + 2.159 \times \text{Cl}^- - 0.224 \times \text{SO}_4^{2-} - 154.923 \quad (4)$$

where NO_3^- , SO_4^{2-} , NH_4^+ , and Cl^- correspond to their respective concentrations ($\mu\text{g}/\text{m}^3$). To validate the applicability of Equation 4 for annual NH_3 estimation and pH simulation in Zhengzhou, this study utilized both observed NH_3 data (from a Thermo Scientific URG-9000D ambient ion monitor, USA) and calculated NH_3 values derived from Equation 4 at the same monitoring site throughout 2022, inputting them into the thermodynamic model for pH simulation. As shown in Figure S2, pH values calculated from observed and simulated NH_3 exhibit good agreement ($r = 0.97$, $P < 0.01$). Furthermore, NH_3 concentrations modeled by ISORROPIA demonstrate a significant correlation ($r = 0.95$, $P < 0.01$) with that simulated NH_3 by Equation 4. These results collectively demonstrate the reliability of the NH_3 estimation method in this study.

2.2.3 HYSPLIT analysis

Backward trajectories were calculated using the mixed-particle Lagrangian integrated trajectory method (HYSPLIT, https://www.ready.noaa.gov/HYSPLIT_traj.php). Meteorological input data were from the Global Data Assimilation System (GDAS) with 3D wind vectors, temperature, relative humidity, geopotential height, surface pressure, and boundary layer diagnostics. 24-h backward trajectories were simulated for air masses above 1000 m above ground level in Zhengzhou. While the surface elevation of Zhengzhou is approximately 100 m above sea level (ASL), setting the height at 1000 m ASL takes into account the minimum altitude needed to traverse the average elevation of the Taihang Mountains (ranging from 1000 to 1500 m ASL). This ensures that the simulated trajectory paths over this topographical barrier are physically realistic.

189 The Angle Distance algorithm was used to cluster air mass trajectories, enabling the identification
190 of dominant air mass directions and potential pollution sources affecting the study site during different
191 periods. The optimal number of clusters was determined by evaluating the spatial variance (SPVAR)
192 of each trajectory from the cluster mean and the total spatial variance (TSV). The final classification
193 was selected just before the second rapid increase in TSV. The underlying principle is that TSV initially
194 rises sharply during clustering, then increases gradually; however, once the number of clusters reaches
195 a certain threshold, TSV surges again, indicating that the merged clusters are highly dissimilar, marking
196 the end of the classification process. The classification results correspond to the different air mass
197 categories before this final merging step. The mean trajectories of these clusters represent the primary
198 airflow patterns at the target site during the analysis period (Wang et al., 2009). Subsequently,
199 trajectories from two periods, 2013–2018 and 2019–2022, were clustered separately to analyze the
200 variations between the two policy implementation periods.

201 **3 Results and discussion**

202 **3.1 Temporal variations in chemical components**

203 Over the past twelve years, the Chinese government implemented the Air Pollution Prevention
204 and Control Action Plans (2013–2018) and the Three-Year Action Plan (2018–2020). The Air Pollution
205 Prevention and Control Action Plan focused on reducing PM_{2.5} concentrations in key regions and
206 aiming to cut PM_{2.5} levels by 10–25% in priority areas over five years. To achieve these goals, it
207 adopted several measures. In terms of industrial restructuring, it mandated the elimination of a large
208 amount of outdated production capacity in industries such as iron/steel and cement to optimize the

209 industrial structure and reduce high-pollution production. For emission standards, it set strict
210 requirements for multiple industrial sectors, especially coal-fired power plants, and gradually
211 introduced ultra-low emission requirements to control pollutants like SO₂, NO_x, and PM. Regarding
212 energy transition, it promoted a shift from coal to cleaner energy sources, including capping coal
213 consumption in certain regions and restricting the construction of small-scale coal-fired boilers.
214 Subsequently, the Three-Year Action Plan was carried out to continue improving air quality with a
215 broader scope of regions under control, further reducing pollutant emissions and enhancing the overall
216 air quality index. The measures included enhanced transportation controls, such as introducing stricter
217 vehicle emission standards (like National VI standards for vehicles) and establishing diesel truck
218 exclusion zones in many cities to reduce emissions from the transportation sector. It also adopted
219 precision governance through grid-based environmental supervision, dividing areas into small grids
220 for more accurate and efficient monitoring of pollution sources. Additionally, it strengthened the legal
221 and institutional framework by revising relevant laws, such as the Air Pollution Prevention and Control
222 Law, to strengthen legal penalties for environmental violations and implementing an environmental
223 tax system to encourage enterprises to reduce emissions.

224 The long-term trends in PM_{2.5} concentrations and its chemical components in Zhengzhou from
225 2011 to 2022 are depicted in Fig. 1, with annual average concentrations listed in Table 1.
226 Correspondingly, the annual average concentration of PM_{2.5} in Zhengzhou decreased from 162 ± 81
227 $\mu\text{g}/\text{m}^3$ in 2011 to $60 \pm 41 \mu\text{g}/\text{m}^3$ in 2022, representing a reduction of approximately 63%. In particular,
228 the reduction rate reached 72% after 2013. As for chemical components, the largest reductions were
229 observed in SO₄²⁻ (79%), decreasing from $38.0 \pm 19.9 \mu\text{g}/\text{m}^3$ in 2013 to $7.9 \pm 4.5 \mu\text{g}/\text{m}^3$ in 2022,

230 followed by EC (76%). Additionally, the concentrations of NH_4^+ and NO_3^- also significantly decreased
231 by 68% and 56%, respectively. The proportion of each component in $\text{PM}_{2.5}$ (Fig. S3) reveals a decrease
232 in SO_4^{2-} , K^+ , and Cl^- , indicating effective control measures targeting coal and biomass combustion
233 (Lei et al., 2021). However, the proportions of NO_3^- and OC in $\text{PM}_{2.5}$ rose from 11% and 12% in 2013
234 to 13% and 17% in 2022, respectively, similar to the trend observed in the North China Plain (Wen et
235 al., 2018; Zhai et al., 2019; Li et al., 2023).

236 3.2 Temporal variations in CM

237 Notably, there is no clear declining trend in the CM concentration, with a rebound observed during
238 2020–2022 (Fig. 1i). Furthermore, the proportion of CM in $\text{PM}_{2.5}$ exhibits a significant upward trend
239 (Fig. S3). To further analyze its trend, sampling data were divided into three periods corresponding to
240 governmental stages: 2011–2013, when no special control measures were implemented; 2013–2019,
241 coinciding with the implementation of the Air Pollution Prevention and Control Action Plan; and
242 2019–2022, coinciding with the Three-Year Action Plan. During these periods, Henan Province and
243 Zhengzhou City implemented several dust control policies summarized in Table S3. As shown in Fig.
244 2a and 2b, the mass concentration of CM peaked at $14.6 \pm 8.3 \mu\text{g}/\text{m}^3$ in 2013, accounting for 8% of
245 $\text{PM}_{2.5}$. To evaluate the inter - annual change trend of CM, the Mann - Kendall method, Sen's slope,
246 and Least - Squares (LS) slope were comprehensively used with the results presented in Table S4.
247 From 2013 to 2019, the CM concentration notably decreased from 14.6 ± 8.3 to $8.5 \pm 7.8 \mu\text{g}/\text{m}^3$, with
248 an annual average decline rate of $0.81 \mu\text{g}/(\text{m}^3 \cdot \text{year})$ from LS slope [$0.015 \mu\text{g}/(\text{m}^3 \cdot \text{year})$ from Sen's
249 slope]. Apart from control measures, the interannual meteorological analysis shows (Fig. S4) WS

exhibited a declining trend, with a decrease rate of 43%, while RH showed an increasing trend at a rate of 8% from 2013 to 2019, under which conditions that were unfavorable for dust resuspension (Wang et al., 2013, 2018). Seasonal trends (Fig. S5) reveal significant declines in CM during spring in 2013–2019 with WS decreasing from 2.2 m/s in 2013 to 1.4 m/s in 2019 (Fig. S6) and stable RH (Fig. S7). Similarly, summer CM reductions in 2013–2019 corresponded with WS declines. These patterns suggest spring-summer CM improvements resulted from the synergistic effects of meteorological changes and dust control policies. Conversely, autumn-winter seasons showed limited CM reductions despite comparable WS decreases in 2013–2019, highlighting the need for enhanced dust emission controls in Zhengzhou during these seasons. As for the individual crustal elements in Fig. S8, Ca exhibited the highest average annual decline rate of 33% during 2013–2019, followed by Al. Si showed a less pronounced decline, attributed to its association with soil dust, where control measures for exposed soil are lacking (Zhang et al., 2020). In addition, the Ca^{2+} concentration as depicted in Fig. 2c decreased from $3.2 \pm 2.1 \mu\text{g}/\text{m}^3$ in 2013 to $2.2 \pm 1.1 \mu\text{g}/\text{m}^3$ in 2019, with an approximate annual average decline rate of $0.32 \mu\text{g}/(\text{m}^3 \cdot \text{year})$ from LS slope [$4.14\text{E}-03 \mu\text{g}/(\text{m}^3 \cdot \text{year})$ from Sen's slope] in Table S4, further demonstrating the decline in dust source. It was worth noting that the proportions of CM, Ca, Al, Fe, Si, and Ca^{2+} in $\text{PM}_{2.5}$ have shown consecutive annual increases from 2013 to 2019, with CM proportion increasing from 8% in 2013 to 14% in 2019, indicating that CM reduction lagged behind $\text{PM}_{2.5}$ reduction efforts in Zhengzhou during this period. Additionally, both concentration and proportion of Ca^{2+} in 2022 ($2.2 \pm 1.1 \mu\text{g}/\text{m}^3$ and 14%) were higher than in other cities of China, such as Beijing ($1.0 \mu\text{g}/\text{m}^3$ and 2.8%), Tianjin ($0.5 \mu\text{g}/\text{m}^3$ and 1.4%), and Xiamen ($0.48 \mu\text{g}/\text{m}^3$ and 1.5%) (Shi et al., 2017; Xu et al., 2025; Zhang et al., 2021). These results indicate that CM remained an

271 important component of PM_{2.5} in Zhengzhou City.

272 During 2019–2022, both CM and Ca²⁺ concentrations exhibited significant rebounds, with annual
273 growth rates of 0.24 and 0.4 µg/(m³·year) from LS slope [5.80E–03 and 5.42E–03 µg/(m³·year) from
274 Sen's slope], respectively, and their proportions increased from 14% and 2% in 2019 to 22% and 5%
275 in 2022. CM concentrations rebounded in all seasons, particularly in winter (Fig. S5). Changes in
276 meteorological conditions may be a significant factor contributing to these concentration rebounds,
277 accompanied by the average WS increased by 0.14 m/s and RH decreased by 7% from 2020 to 2022
278 (Fig. S4, S6, and S7), facilitating dust resuspension. Furthermore, the lack of more effective dust
279 control measures, as indicated by the absence of significant changes in the dust control policies from
280 the Air Pollution Prevention and Control Action Plan and Three-Year Action Plan, may be another
281 important factor contributing to the rebound of dust.

282 3.3 Sources of CM

283 Elemental ratios were employed to characterize the sources of CM, with the Ca/Al ratio widely
284 recognized as a reliable indicator of sandy origin (Zhang et al., 2017). In addition, significant variations
285 in Ca/Si ratios (Table S5) were observed among different dust sources (Road, Construction, Piles, Soil).
286 Fig. 3a illustrates the trend in Ca/Si ratios from 2011 to 2022. After 2013, Ca/Si ratios showed a
287 declining trend annually, with the average ratio decreasing from a peak of 1.6 in 2016 to a lowest of
288 0.4 in 2022. Compared with Ca/Si ratios from different types of dust sources, the effect of road and
289 construction dust on CM has gradually decreased. This may be attributed to the implementation of dust
290 control measures such as enclosure, shielding, and dust suppression at construction and demolition

291 sites, as well as dust control on ground surfaces and roads (Table S5). During 2019–2022, the average
292 Ca/Si ratio remained below 1, with a mean of 0.4 in 2022, indicating that soil dust predominantly
293 contributed to CM. Currently, measures for controlling soil-suspended dust are limited, primarily
294 relying on long-term strategies such as afforestation and increasing urban green coverage, thus
295 requiring a longer process and sustained investment.

296 Sand dust transport serves as a significant source of CM in the North China Plain (Zhang et al.,
297 2024). The Ca/Al ratio from 2016 to 2022 (Fig. 3b) shows minimal variation, with annual averages
298 ranging between 1.5 and 2.5, indicating no significant changes in the source regions of sand. The
299 transport trajectories reveal that the predominant pathways for long-distance transport of sand dust
300 originated from Inner Mongolia, passing through Shaanxi and Shanxi provinces. Compared to 2013–
301 2018 (45%), the influence of long-distance transport decreased to 25% during 2019–2022. In contrast,
302 local transport within Henan province and short-distance transport from Shandong province showed a
303 noticeable increase. These findings suggest that the rebound in CM concentrations during 2019–2022
304 in Zhengzhou might be responsible for the resuspension of surrounding soil dust.

305 3.4 Long-term trend of particle pH

306 Are shown in Fig. 4 and Table S4, pH values showed a clearly increasing trend after 2014. From
307 2013 to 2019, the annual pH increased by 0.11 units from the LS slope [9.15E–04 units from Sen’s
308 slope], reaching a maximum median value of 4.45 (Mean: 4.35) in 2018. Note that the annual average
309 growth rate of pH values increased to 0.21 units from LS slope [2.93E–03 units from Sen’s slope] from
310 2019 to 2022, with a maximum median value of 4.42 (Mean: 4.51) in 2022. Seasonally, pH values

311 showed increasing trends in spring, summer, and autumn, and notably increased in winter from 2020
312 to 2022 (Fig. S9). The increasing trend in pH values observed in this study is similar to the findings in
313 Beijing (Song et al., 2019; Xie et al., 2020), presumably attributable to the comparable chemical
314 composition trends and meteorological conditions. In contrast, Shanghai and Hong Kong display
315 divergent trends (Nah et al., 2023; Zhou et al., 2022). This disparity might be ascribed to the stronger
316 buffering effect exerted by NH_3 and dust in Zhengzhou than marine aerosols (Na^+/Cl^-) in these coastal
317 cities (Shi et al., 2017; Liu et al., 2019). Moreover, the relatively higher temperatures and more
318 abundant rainfall in Shanghai and Hong Kong could also contribute to the distinct trends observed in
319 their pH values.

320 Sensitivity analyses were conducted to explore the dominant factors driving the elevated particle
321 pH in Zhengzhou by giving a range for one parameter (i.e., TNH_x) and average values for other
322 parameters (i.e., SO_4^{2-} , NO_3^- , Na^+ , Cl^- , Ca^{2+} , K^+ , Mg^{2+} , RH, and T) input into the ISORROPIA-II model.

323 Are shown in Fig. S10, particle pH increases with the cation concentrations (e.g., TNH_x , K^+ , Ca^{2+} ,
324 Mg^{2+} , and Na^+) and decreases with anions concentrations (e.g., SO_4^{2-} and NO_3^-). Additionally, RH
325 does not significantly affect pH, whereas an increase in T leads to a noticeable decrease in particle pH.

326 Based on the sensitivity analysis curves, the pH values corresponding to a variable in different
327 years were calculated according to the average values of this variable in different years (Table S6). The
328 difference in pH values of this variable between two adjacent years was defined as ΔpH which is
329 illustrated in Fig. 5. According to Equation (2), in addition to H^+ concentration, particle pH is primarily
330 influenced by the dilution effect of ALWC. Moreover, ALWC affects the gas-particle partitioning of
331 semi-volatile compounds, thereby influencing particle acidity (Zuend et al., 2010; Zuend and Seinfeld,

2012). As shown in Fig.5 and Table S6, only in 2015, 2019, and 2020 did the increases in ALWC concentration ($17.6 \mu\text{g}/\text{m}^3$, $4.1 \mu\text{g}/\text{m}^3$, and $11.6 \mu\text{g}/\text{m}^3$, respectively) lead to pH increases of 0.22, 0.06, and 0.14 units. This clearly cannot fully explain the significant pH increase in Zhengzhou since 2013. Notably, since 2013, H^+ concentration has shown a decreasing trend. Particularly, H^+ concentrations decreased by 7.6×10^{-6} , 11.2×10^{-6} , and $7.2 \times 10^{-6} \text{ mol/L}$ in 2013, 2015, and 2017, respectively, leading to pH increases of 0.21, 0.36, and 0.42 units. After 2019, a continuous decline in H^+ concentration was observed for three consecutive years, resulting in pH increases of 0.21, 0.13, and 0.2 units in 2020, 2021, and 2022, respectively. These findings indicate that the increase in pH from 2019 to 2022 in Zhengzhou was primarily driven by the reduction in H^+ concentration.

The concentration of H^+ in the aerosol liquid phase is influenced by both chemical composition and meteorological conditions. To further understand the factors affecting ΔpH , we analyzed the variations in $\text{PM}_{2.5}$ chemical components and meteorological parameters. Results indicate that the decline in SO_4^{2-} from 2013 to 2018 was the primary cause of the increase in particle pH, as it decreased H^+ and ALWC concentrations (Fig. S11) in aerosol (Ding et al., 2019; Zhang et al., 2021). The average SO_4^{2-} concentration decreased by 14.6 and $5.3 \mu\text{g}/\text{m}^3$, resulting in a pH increase of 0.43 and 0.35 units from 2013 to 2014 and 2016 to 2017, respectively, which was comparable to an increased rate of 0.3 units in East Asia due to SO_2 emission controls since 2016 (Karydis et al., 2021). As another acidic ion, the decrease in nitrate concentration did not significantly contribute to the pH increases, consistent with findings from Ding et al. (2019) and Zhang et al. (2021). This is primarily because NO_3^- declined more slowly compared to sulfate ions and exceeded sulfate concentrations after 2016, under which conditions that nitrate-rich particles can absorb twice the amount of water that sulfate-rich particles,

353 leading to an increase in ALWC concentration and inhibiting pH decline (Lin et al., 2020; Xie et al.,
354 2020). On the other hand, increases in particle pH in 2015 and 2018 were notably influenced by
355 changes in TNH_x with concentrations increased by 5.5 and 1.3 $\mu\text{g}/\text{m}^3$, respectively. Increased TNH_x
356 concentrations could react with SO_4^{2-} or NO_3^- and consume a substantial amount of H^+ , thereby raising
357 particulate matter pH values (Seinfeld et al., 1998; Zhang et al., 2021). Substantial decreases in T in
358 2015 (4.2°C), 2017 (4.9°C), and 2018 (2.8°C), favoring NH_3 partitioning into the particle phase and
359 reducing H^+ concentrations, drove increases in particle pH (Tao and Murphy, 2019).

360 During the period from 2020 to 2022, the influence of SO_4^{2-} on particle pH gradually decreased,
361 with a decrease in concentration from 0.3 to 2.3 $\mu\text{g}/\text{m}^3$ (Table S6) only bringing about a pH decrease
362 of 0.03 to 0.14 (Fig. 5). Moreover, a rebound in SO_4^{2-} concentration to $7.9 \pm 4.5 \mu\text{g}/\text{m}^3$ in 2022 even
363 resulted in a decrease of 0.11 units in pH instead. On the other hand, TNH_x began to show a slight
364 annual decline (0.9 to 2.2 $\mu\text{g}/\text{m}^3$), resulting in a significant decrease in pH (0.21–0.35). Consequently,
365 the increase in pH values was closely related to the rise in Ca^{2+} concentration. Ca^{2+} is less volatile and
366 competes preferentially with NH_3 to neutralize anions such as SO_4^{2-} to form insoluble CaSO_4 , which
367 precipitates from the aerosol aqueous phase (Ding et al., 2019; Karydis et al., 2021), thereby reducing
368 H^+ concentrations (Fig. S11) and subsequently lowering particle acidity. Specifically, increases of 0.7
369 and 0.5 $\mu\text{g}/\text{m}^3$ in Ca^{2+} concentrations led to pH increases of 0.13 and 0.09 units in 2020 and 2022,
370 respectively, making Ca^{2+} a primary controlling factor for pH elevation.

371 4 Conclusions

372 The annual average $\text{PM}_{2.5}$ concentration in Zhengzhou decreased from $212.4 \pm 101.5 \mu\text{g}/\text{m}^3$ in

2013 to $59.5 \pm 41.2 \mu\text{g}/\text{m}^3$ in 2022, with the largest reduction in SO_4^{2-} . As for CM, their concentrations notably decreased from 2013 to 2019, because of effective dust control measures, as well as decreased wind speed and increased relative humidity. However, the proportions of CM in $\text{PM}_{2.5}$ have shown consecutive annual increases. In addition, CM concentrations and their proportions increased significantly during 2019–2022, which might be responsible for the resuspension of surrounding soil dust. Correspondingly, the annual pH increased by 0.11 units from 2013 to 2019 mainly due to the decline in SO_4^{2-} , increased TNH_x , or decreased temperature. During the period from 2020 to 2022, the annual average growth rate of pH values increased to 0.21 units from 2019 to 2022, which was determined by the rise in Ca^{2+} concentration.

5 Implication

Control measures implemented by the Chinese government have proven effective in reducing dust, but this study reveals that the crustal materials in $\text{PM}_{2.5}$ rebounded after 2019. This phenomenon is not unique to Zhengzhou, as major cities in the North China Plain have also experienced a pronounced upward trend in coarse particles after 2019 (Fig. S12). Thus, crustal materials persist as a substantial constituent of atmospheric aerosols in North China, sustaining elevated particle pH levels. Extensive research has established that heightened particle pH inhibits nitrate reduction in aerosols (Ding et al., 2019; Lin et al., 2020; Wen et al., 2018), particularly significant given nitrate's predominant role in haze formation within this region. Notably, while moderately acidic aerosols demonstrate reduced health impacts, particles with $\text{pH} < 3$ exhibit substantially greater health risks (Shi et al., 2019). Consequently, future environmental management strategies must prioritize real-time assessment of

393 regulatory impacts on particle acidity. This necessitates an integrated approach that simultaneously
394 addresses acidic precursors, alkaline precursors, and crustal material contributions to atmospheric acid
395 chemistry.

396 **Data availability**

397 All the data presented in this article can be accessed through
398 <https://doi.org/10.5281/zenodo.14032007> (Zhang, 2024).

399 **Supporting Information**

400 Additional data, figures, and tables, some of which are referenced directly within the manuscript,
401 and detailed descriptions of field measurements and samples.

402 **Author contributions**

403 Shenbo Wang designed this study. Hongyu Zhang and Zhangsen Dong analyzed the data and
404 prepared the manuscript with the contributions of all coauthors. Xiao Li conducted measurements.
405 Ruiqin Zhang provided funding acquisition. All authors have read and agreed to the published version
406 of the manuscript.

407 **Competing interests**

408 The authors declare that they have no conflict of interest.

409 **Acknowledgment**

410 This work was supported by the National Key Research and Development Program of China (No.
411 2024YFC3713701), the China Postdoctoral Science Foundation (2023 M733220), the Zhengzhou
412 PM_{2.5} and O₃ Collaborative Control and Monitoring Project (20220347 A), and the National Key R&D
413 Program of China No. 2017YFC0212400.

414 **Funding Sources**

415 This work was supported by the National Key Research and Development Program of China (No.
416 2024YFC3713701), the China Postdoctoral Science Foundation (2023 M733220), the Zhengzhou
417 PM_{2.5} and O₃ Collaborative Control and Monitoring Project (20220347 A), and the National Key
418 Research and Development Program of China (No. 2017YFC0212400).

419 **References**

- 420 Battaglia, M. A.; Douglas, S.; Hennigan, C.: Effect of the urban heat island on aerosol pH, Environ.
421 Sci. Technol., 51, 13095–13103, <https://doi.org/10.1021/acs.est.7b02786>, 2017.
- 422 Chang, R. Y. W.; Slowik, J. G.; Shantz, N. C.; Vlasenko, A.; Liggio, J.; Sjostedt, S. J.; Leaitch, W. R.;
423 Abbatt, J. P. D. The hygroscopicity parameter (κ) of ambient organic aerosol at a field site subject
424 to biogenic and anthropogenic influences: relationship to degree of aerosol oxidation. Atmos.
425 Chem. Phys., 10, 5047–5064, <https://doi.org/10.5194/acp-10-5047-2010>, 2010.
- 426 Ding, J., Zhao, P., Su, J., Dong, Q., Du, X., and Zhang, Y.: Aerosol pH and its driving factors in Beijing,
427 Atmos. Chem. Phys., 19, 7939–7954, <https://doi.org/10.5194/acp-19-7939-2019>, 2019.
- 428 Dong, J., Li, B., Li, Y., Zhou, R., Gan, C., Zhao, Y., Liu, R., Yang, Y., Wang, T., and Liao, H.:

429 Atmospheric ammonia in China: Long-term spatiotemporal variation, urban-rural gradient, and
 430 influencing factors, *Sci. Total Environ.*, 883, 163733,
 431 <https://doi.org/10.1016/j.scitotenv.2023.163733>, 2023.

432 Fountoukis, C and Nenes, A.: ISORROPIA II: a computationally efficient thermodynamic equilibrium
 433 model for K^+ - Ca^{2+} - Mg^{2+} - NH_4^+ - Na^+ - SO_4^{2-} - NO_3^- - Cl^- - H_2O aerosols, *Atmos. Chem. Phys.*,
 434 7, 4639–4659, <https://doi.org/10.5194/acp-7-4639-2007>, 2007.

435 Guo, H., Sullivan, A. P., Campuzano-Jost, P., Schroder, J. C., Lopez-Hilfiker, F. D., Dibb, J. E., Jimenez,
 436 J. L., Thornton, J. A., Brown, S. S., Nenes, A., and Weber, R. J.: Fine particle pH and the
 437 partitioning of nitric acid during winter in the northeastern United States, *J. Geophys. Res. Atmos.*,
 438 121, 10,355–310,376, <https://doi.org/10.1002/2016JD025311>, 2016.

439 Guo, H., Xu, L., Bougiatioti, A., Cerully, K. M., Capps, S. L., Hite Jr, J. R., Carlton, A. G., Lee, S. H.,
 440 Bergin, M. H., Ng, N. L., Nenes, A., and Weber, R. J.: Fine-particle water and pH in the
 441 southeastern United States, *Atmos. Chem. Phys.*, 15, 5211–5228, [https://doi.org/10.5194/acp-15-](https://doi.org/10.5194/acp-15-5211-2015)
 442 [5211-2015](https://doi.org/10.5194/acp-15-5211-2015), 2015.

443 Heald, C.; Collett, J. J.; Lee, T.; Benedict, K.; Schwandner, F.; Li, Y.; Clarisse, L.; Hurtmans, D. R.;
 444 Van, D. M.; Clerbaux, C.; Coheur, P. F., Philip, S.; Martin, R. V.; Pye, T.: Atmospheric ammonia
 445 and particulate inorganic nitrogen over the United States, *Atmos. Chem. Phys.*, 12, 10295–10312,
 446 <https://doi.org/10.5194/acp-12-10295-2012>, 2012.

447 Huang, X., Song, Y., Li, M., Li, J., Huo, Q., Cai, X., Zhu, T., Hu, M., and Zhang, H.: A high-resolution
 448 ammonia emission inventory in China, *Global. Biogeochem. Cy.*, 26, GB1030,
 449 <https://doi.org/10.1029/2011GB004161>, 2012.

450 Jiang, N.; Duan, S.; Yu, X.; Zhang, R.; Wang, K. Comparative major components and health risks of
 451 toxic elements and polycyclic aromatic hydrocarbons of $PM_{2.5}$ in winter and summer in
 452 Zhengzhou: Based on three-year data. *Atmos. Res.*, 213, 173–184,
 453 <https://doi.org/10.1016/j.atmosres.2018.06.008>, 2018.

454 Karydis, V. A., Tsimpidi, A. P., Pozzer, A., and Lelieveld, J.: How alkaline compounds control
 455 atmospheric aerosol particle acidity, *Atmos. Chem. Phys.*, 21, 14983–15001,
 456 <https://doi.org/10.5194/acp-21-14983-2021>, 2021.

Kim, Y., Park, O., Park, S. H., Kim, M. J., Kim, J.-J., Choi, J.-Y., Lee, D., Cho, S., and Shim, S.: PM_{2.5} pH estimation in Seoul during the KORUS-AQ campaign using different thermodynamic models, *Atmos. Environ.*, 268, 118787, <https://doi.org/10.1016/j.atmosenv.2021.118787>, 2022.

Lei, L., Zhou, W., Chen, C., He, Y., Li, Z., Sun, J., Tang, X., Fu, P., Wang, Z., and Sun, Y.: Long-term characterization of aerosol chemistry in cold season from 2013 to 2020 in Beijing, China, *Environ. Pollut.*, 268, 115952, <https://doi.org/10.1016/j.envpol.2020.115952>, 2021.

Li, C.; Hu, Y.; Chen, J.; Ma, Z.; Ye, X.; Yang, X.; Wang, L.; Wang, X.; Mellouki, A. Physiochemical properties of carbonaceous aerosol from agricultural residue burning: Density, volatility, and hygroscopicity. *Atmos. Environ.*, 140, 94–105, <https://doi.org/10.1016/j.atmosenv.2016.05.052>, 2016.

Li, W., Xu, L., Liu, X., Zhang, J., Lin, Y., Yao, X., Gao, H., Zhang, D., Chen, J., Wang, W., Harrison, R. M., Zhang, X., Shao, L., Fu, P., Nenes, A., and Shi, Z.: Air pollution-aerosol interactions produce more bioavailable iron for ocean ecosystems, *Sci. Adv.*, 3, e1601749, <https://doi.org/10.1126/sciadv.1601749>, 2017.

Li, Y., Lei, L., Sun, J., Gao, Y., Wang, P., Wang, S., Zhang, Z., Du, A., Li, Z., Wang, Z., Kim, J. Y., Kim, H., Zhang, H., and Sun, Y.: Significant reductions in secondary aerosols after the Three-Year Action Plan in Beijing summer, *Environ. Sci. Technol.*, 57, 15945–15955, <https://doi.org/10.1021/acs.est.3c02417>, 2023.

Lin, Y., Zhang, Y., Fan, M., and Bao, M.: Heterogeneous formation of particulate nitrate under ammonium-rich regimes during the high-PM_{2.5} events in Nanjing, China, *Atmos. Chem. Phys.*, 20, 3999–4011, <https://doi.org/10.5194/acp-20-3999-2020>, 2020.

Liu, M.; Huang, X.; Song, Y.; Tang, J.; Cao, J.; Zhang, X.; Zhang, Q.; Wang, S.; Xu, T.; Kang, L.; Gai, X.; Zhang, H.; Yang, F.; Wang, H.; Yu, J.; Lau, A.; He, L.; Huang, X.; Duan, L.; Ding, A.; Xue, L.; Gao, J.; Liu, B.; Zhu, T. Ammonia emission control in China would mitigate haze pollution and nitrogen deposition, but worsen acid rain. *Proc. Natl. Acad. Sci.*, 116, 7760–7765, <https://doi.org/10.1073/pnas.1814880116>, 2019.

Liu, Z., Gao, W., Yu, Y., Hu, B., Xin, J., Sun, Y., Wang, L., Wang, G., Bi, X., Zhang, G., Xu, H., Cong, Z., He, J., Xu, J., and Wang, Y.: Characteristics of PM_{2.5} mass concentrations and chemical species

485 in urban and background areas of China: emerging results from the CARE-China network, *Atmos.*
 486 *Chem. Phys.*, 18, 8849–8871, <https://doi.org/10.5194/acp-18-8849-2018>, 2018.

487 Mao, I., Lin, C., Lin, C., Chen, Y., Sung, F., and Chen, M.: Exposure of acid aerosol for schoolchildr
 488 en in metropolitan Taipei, *Atmos. Environ.*, 43, 5622–5629, [https://doi.org/10.1016/j.atmosenv.2](https://doi.org/10.1016/j.atmosenv.2009.07.054)
 489 [009.07.054](https://doi.org/10.1016/j.atmosenv.2009.07.054), 2009.

490 Masiol, M., Squizzato, S., Formenton, G., Khan, M. B., Hopke, P. K., Nenes, A., Pandis, S. N., Tositti,
 491 L., Benetello, F., Visin, F., and Pavoni, B.: Hybrid multiple-site mass closure and source
 492 apportionment of PM_{2.5} and aerosol acidity at major cities in the Po Valley, *Sci. Total Environ.*,
 493 704, 135287, <https://doi.org/10.1016/j.scitotenv.2019.135287>, 2020.

494 MEP (Ministry of Environment Protection), 2023. [https://www.mee.gov.cn/ywdt/hjywnews/202406/t](https://www.mee.gov.cn/ywdt/hjywnews/202406/t20240605_1075031.shtml)
 495 [20240605_1075031.shtml](https://www.mee.gov.cn/ywdt/hjywnews/202406/t20240605_1075031.shtml), Accessed date:5 June 2024.

496 Nah, T., Lam, Y. H., Yang, J., and Yang, L.: Long-term trends and sensitivities of PM_{2.5} pH and aerosol
 497 liquid water to chemical composition changes and meteorological parameters in Hong Kong,
 498 South China: Insights from 10-year records from three urban sites, *Atmos. Environ.*, 302,
 499 <https://doi.org/10.1016/j.atmosenv.2023.119725>, 2023.

500 Nenes, A., Pandis, S. N., Kanakidou, M., Russell, A. G., Song, S., Vasilakos, P., and Weber, R. J.:
 501 Aerosol acidity and liquid water content regulate the dry deposition of inorganic reactive nitrogen,
 502 *Atmos. Chem. Phys.*, 21, 6023–6033, <https://doi.org/10.5194/acp-21-6023-2021>, 2021.

503 Pinder, R., Adams, P., and Pandis, S.: Ammonia emission controls as a cost-effective strategy for
 504 reducing atmospheric particulate matter in the eastern United States, *Environ. Sci. Technol.*, 41,
 505 380–386, <https://doi.org/10.1021/es060379a>, 2007.

506 Pinder, R., Gilliland, A., and Dennis, R.: Environmental impact of atmospheric NH₃ emissions under
 507 present and future conditions in the eastern United States, *Geophys. Res. Lett.*, 35, 28,
 508 <https://doi.org/10.1029/2008gl033732>, 2008.

509 Pye, H. O. T.; Nenes, A.; Alexander, B.; Ault, A. P.; Barth, M. C.; Clegg, S. L.; Collett Jr, J. L.; Fahey,
 510 K. M.; Hennigan, C. J.; Herrmann, H.; Kanakidou, m.; Kelly, J. T.; Ku, L.; McNeill, V. F.; Riemer,
 511 N.; Schaefer, T.; Shi, G.; Tilgner, A.; Walker, J.T.; Wang, T.; Weber, R.; Xing, J.; Zaveri, R. A.;
 512 Zuend, A. The acidity of atmospheric particles and clouds. *Atmos. Chem. Phys.*, 20, 4809–4888,

513 <https://doi.org/10.5194/acp-20-4809-2020>, 2020.

514 Rengarajan, R., Sudheer, A. K., and Sarin, M. M.: Aerosol acidity and secondary organic aerosol
 515 formation during wintertime over urban environment in western India, *Atmos. Environ.*, 45,
 516 1940–1945, <https://doi.org/10.1016/j.atmosenv.2011.01.026>, 2011.

517 Seinfeld, J. H., Pandis, S. N., and Noone, K. J.: Atmospheric chemistry and physics: From air pollution
 518 to climate change, *Phys. Today.*, 51, 88–90, <https://doi.org/10.1063/1.882420>, 1998.

519 Sharma, B., Jia, S., Polana, A. J., Ahmed, M. S., Haque, R. R., Singh, S., Mao, J., and Sarkar, S.:
 520 Seasonal variations in aerosol acidity and its driving factors in the eastern Indo-Gangetic Plain:
 521 A quantitative analysis, *Chemosphere.*, 305, 135490,
 522 <https://doi.org/10.1016/j.chemosphere.2022.135490>, 2022.

523 Shi, G., Xu, J., Peng, X., Xiao, Z., Chen, K., Tian, Y., Guan, X., Feng, Y., Yu, H., Nenes, A., and Russell,
 524 A. G.: pH of aerosols in a polluted atmosphere: source contributions to highly acidic aerosol,
 525 *Environ. Sci. Technol.*, 51, 4289–4296, <https://doi.org/10.1021/acs.est.6b05736>, 2017.

526 Shi, X., Nenes, A., Xiao, Z., Song, S., Yu, H., Shi, G., Zhao, Q., Chen, K., Feng, Y., and Russell, A. G.:
 527 High-resolution data sets unravel the effects of sources and meteorological conditions on nitrate
 528 and its gas-particle partitioning, *Environ. Sci. Technol.*, 53, 3048–3057,
 529 <https://doi.org/10.1021/acs.est.8b06524>, 2019.

530 Song, S., Nenes, A., Gao, M., Zhang, Y., Liu, P., Shao, J., Ye, D., Xu, W., Lei, L., Sun, Y., Liu, B.,
 531 Wang, S., and McElroy, M. B.: Thermodynamic modeling suggests declines in water uptake and
 532 acidity of inorganic aerosols in Beijing winter haze events during 2014/2015–2018/2019, *Environ.*
 533 *Sci. Technol. Lett.*, 6, 752–760, <https://doi.org/10.1021/acs.estlett.9b00621>, 2019.

534 Su, H., Cheng, Y., and Pöschl, U.: New Multiphase Chemical Processes Influencing Atmospheric
 535 Aerosols, Air Quality, and Climate in the Anthropocene, *Acc. Chem. Res.*, 53, 2034–2043,
 536 <https://doi.org/10.1021/acs.accounts.0c00246>, 2020.

537 Surratt, J. D., Chan, A. W. H., Eddingsaas, N. C., Chan, M., Loza, C. L., Kwan, A. J., Hersey, S. P.,
 538 Flagan, R. C., Wennberg, P. O., and Seinfeld, J. H.: Reactive intermediates revealed in
 539 secondary organic aerosol formation from isoprene, *Proc. Natl. Acad. Sci.*, 107, 6640–6645,
 540 <https://doi.org/10.1073/pnas.0911114107>, 2010.

541 Tao, Y. and Murphy, J. G.: The sensitivity of PM_{2.5} acidity to meteorological parameters and chemical
542 composition changes: 10-year records from six Canadian monitoring sites, *Atmos. Chem. Phys.*,
543 19, 9309–9320, <https://doi.org/10.5194/acp-19-9309-2019>, 2019.

544 Tian, Y.; Chen, G.; Wang, H.; Huang-Fu, Y.; Shi, G.; Han, B.; and Feng, Y.: Source regional
545 contributions to PM_{2.5} in a megacity in China using an advanced source regional apportionment
546 method. *Chemosphere.*, 147, 256–263, <https://doi.org/10.1016/j.chemosphere.2015.12.132>, 2016.

547 Tremper, A.; Font, A.; Priestman, M.; Hamad, S.; Chung, T.; Pribadi, A.; Brown, R.; Goddard, S.;
548 Grassineau, N.; Petterson, K.; Kelly, F.; Green, D.: Field and laboratory evaluation of a high time
549 resolution x-ray fluorescence instrument for determining the elemental composition of ambient
550 aerosols, *Atmos. Meas. Tech.*, 11, 3541–3557, <https://doi.org/10.5194/amt-11-3541-2018>, 2018.

551 Wang, C., Yin, S., Bai, L., Zhang, X., Gu, X., Zhang, H., Lu, Q., and Zhang, R.: High-resolution
552 ammonia emission inventories with comprehensive analysis and evaluation in Henan, China,
553 2006–2016, *Atmos. Environ.*, 193, 11–23, <https://doi.org/10.1016/j.atmosenv.2018.08.063>, 2018.

554 Wang, G., Chen, J., Xu, J., Yun, L., Zhang, M., Li, H., Qin, X., Deng, C., Zheng, H., Gui, H., Liu, J.,
555 and Huang, K.: Atmospheric processing at the Sea-Land interface over the South China Sea:
556 Secondary aerosol formation, aerosol acidity, and role of sea salts, *J. Geophys. Res. Atmos.*,
557 127, <https://doi.org/10.1029/2021jd036255>, 2022.

558 Wang, L., Du, H., Chen, J., Zhang, M., Huang, X., Tan, H., Kong, L., and Geng, F.: Consecutive
559 transport of anthropogenic air masses and dust storm plume: Two case events at Shanghai, China,
560 *Atmos. Res.*, 127, 22–33, <https://doi.org/10.1016/j.atmosres.2013.02.011>, 2013.

561 Wang, S., Yin, S., Zhang, R., Yang, L., Zhao, Q., Zhang, L., Yan, Q., Jiang, N., and Tang, X.: Insight
562 into the formation of secondary inorganic aerosol based on high-time-resolution data during haze
563 episodes and snowfall periods in Zhengzhou, China, *Sci. Total Environ.*, 660, 47–56,
564 <https://doi.org/10.1016/j.scitotenv.2018.12.465>, 2019.

565 Wang, S.; Wang, L.; Li, Y.; Wang, C.; Wang, W.; Yin, S.; Zhang, R.: Effect of ammonia on fine-particle
566 pH in agricultural regions of China: comparison between urban and rural sites, *Atmos. Chem.*
567 *Phys.*, 20, 2719–2734, <https://doi.org/10.5194/acp-20-2719-2020>, 2020.

568 Wang, Y., Zhang, X., and Draxler, R.: TrajStat: GIS-based software that uses various trajectory

569 statistical analysis methods to identify potential sources from long-term air pollution
 570 measurement data, *Environ. Model. Softw.*, 24, 938–939,
 571 <https://doi.org/10.1016/j.envsoft.2009.01.004>, 2009.

572 Wang, Z., Pan, X., Uno, I., Chen, X., Yamamoto, S., Zheng, H., Li, J., and Wang, Z.: Importance of
 573 mineral dust and anthropogenic pollutants mixing during a long-lasting high PM event over East
 574 Asia, *Environ. Pollut.*, 234, 368–378, <https://doi.org/10.1016/j.envpol.2017.11.068>, 2018.

575 Weber, R.; Guo, H.; Russell, A.; Nenes, A.: High aerosol acidity despite declining atmospheric sulfate
 576 concentrations over the past 15 years, *Nature Geoscience.*, 9, 282–285,
 577 <https://doi.org/10.1038/ngeo2665>, 2016.

578 Wei, Y.; Wang, S.; Jiang, N.; Zhang, R.; and Hao, Q. Comparative multi-model study of PM_{2.5} acidity
 579 trend changes in ammonia-rich regions in winter: Based on a new ammonia concentration
 580 assessment method, *J. Hazard.*, 458, 15, <https://doi.org/10.1016/10.1016/j.jhazmat.2023.131970>,
 581 2023.

582 Wen, L., Xue, L., Wang, X., Xu, C., Chen, T., Yang, L., Wang, T., Zhang, Q., and Wang, W.:
 583 Summertime fine particulate nitrate pollution in the North China Plain: increasing trends,
 584 formation mechanisms and implications for control policy, *Atmos. Chem. Phys.*, 18, 11261–
 585 11275, <https://doi.org/10.5194/acp-18-11261-2018>, 2018.

586 Wexler, A. S. and Seinfeld, J. H.: Second-generation inorganic aerosol model, *Atmos. Environ., Part*
 587 *A. General Topics*, 25, 2731–2748, [https://doi.org/10.1016/0960-1686\(91\)90203-J](https://doi.org/10.1016/0960-1686(91)90203-J), 1991.

588 Xie, Y., Wang, G., Wang, X., Chen, J., Chen, Y., Tang, G., Wang, L., Ge, S., Xue, G., Wang, Y., and
 589 Gao, J.: Nitrate-dominated PM_{2.5} and elevation of particle pH observed in urban Beijing during
 590 the winter of 2017, *Atmos. Chem. Phys.*, 20, 5019–5033, [https://doi.org/10.5194/acp-20-5019-](https://doi.org/10.5194/acp-20-5019-2020)
 591 [2020](https://doi.org/10.5194/acp-20-5019-2020), 2020.

592 Xu, K., Yin, L., Chen, Q., Liao, D., Ji, X., Zhang, K., Wu, Y., Xu, L., Li, M., Fan, X., Zhang, F., Huang,
 593 Z., Chen, J., and Hong, Y.: Quantitative analysis of influencing factors to aerosol pH and its
 594 responses to PM_{2.5} and O₃ pollution in a coastal city, *J. Environ. Sci.*, 151, 284–297,
 595 <https://doi.org/10.1016/j.jes.2024.03.044>, 2025.

596 Yu, F., Yan, Q., Jiang, N., Su, F., Zhang, L., Yin, S., Li, Y., Zhang, R., and Chen, L.: Tracking pollutant

597 characteristics during haze events at background site Zhongmu, Henan Province, China, *Atmos.*
 598 *Pollut. Res.*, 8, 64–73, <https://doi.org/10.1016/j.apr.2016.07.005>, 2017.

599 Zhai, S.; Jacob, D.J.; Wang, X.; Shen, L.; Li, K.; Zhang, Y.; Gui, K.; Zhao, T.; Liao, H. Fine particulate
 600 matter (PM_{2.5}) trends in China, 2013–2018: separating contributions from anthropogenic
 601 emissions and meteorology, *Atmos. Chem. Phys.*, 19, 11031–11041, [https://doi.org/10.5194/acp-](https://doi.org/10.5194/acp-19-11031-2019)
 602 [19-11031-2019](https://doi.org/10.5194/acp-19-11031-2019), 2019.

603 Zhang, B., Shen, H., Liu, P., Guo, H., Hu, Y., Chen, Y., Xie, S., Xi, Z., Skipper, T. N., and Russell, A.
 604 G.: Significant contrasts in aerosol acidity between China and the United States, *Atmos. Chem.*
 605 *Phys.*, 21, 8341–8356, <https://doi.org/10.5194/acp-21-8341-2021>, 2021.

606 Zhang, G., Ding, C., Jiang, X., Pan, G., Wei, X., and Sun, Y.: Chemical compositions and sources
 607 contribution of atmospheric particles at a typical steel industrial urban site, *Sci. Rep.*, 10, 7654,
 608 <https://doi.org/10.1038/s41598-020-64519-x>, 2020.

609 Zhang, Z., Dong, Z., Zhang, C., Qian, G., and Lei, C.: The geochemical characteristics of dust material
 610 and dust sources identification in northwestern China, *J. Geochem. Explor.*, 175, 148–155,
 611 <https://doi.org/10.1016/j.gexplo.2016.11.006>, 2017.

612 Zhang, Z., Kuang, Z., Yu, C., Wu, D., Shi, Q., Zhang, S., Wang, Z., and Liu, D.: Trans–boundary dust
 613 transport of dust storms in Northern China: A study utilizing ground–based lidar network and
 614 CALIPSO satellite, *Remote sens.*, 16, 1196, <https://doi.org/10.3390/rs16071196>, 2024.

615 Zheng, G., Su, H., and Cheng, Y.: Revisiting the key driving processes of the decadal trend of aerosol
 616 acidity in the U.S, *Acs. Environ. Au.*, 2, 346–353, <https://doi.org/10.1021/acsenvironau.1c00055>,
 617 2022.

618 Zheng, G., Su, H., Wang, S., Andreae, M. O., Pöschl, U., and Cheng, Y.: Multiphase buffer theory
 619 explains contrasts in atmospheric aerosol acidity, *Science.*, 369, 1374–1377,
 620 <https://doi.org/10.1126/science.aba3719>, 2020.

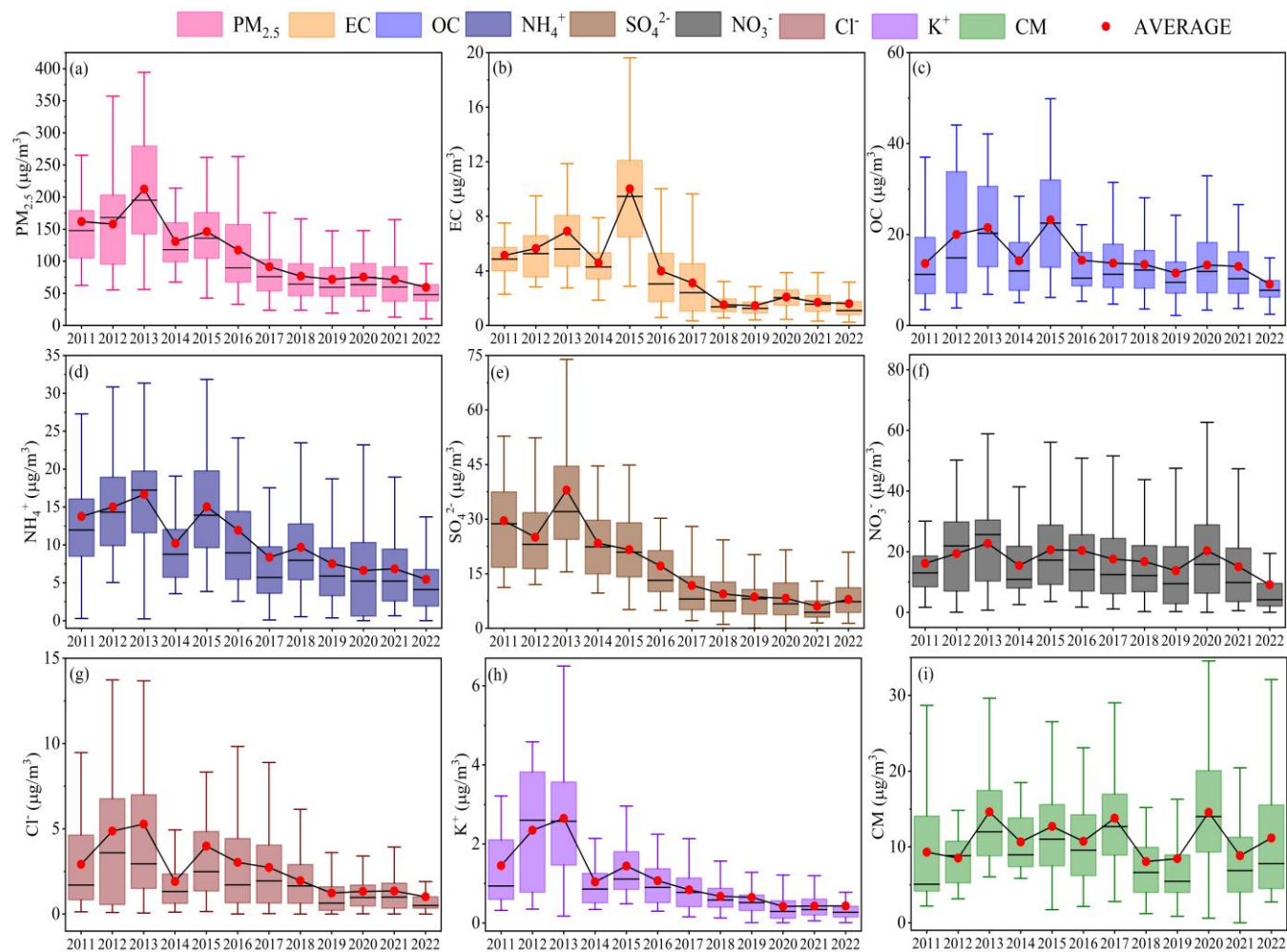
621 Zhou, M., Zheng, G., Wang, H., Qiao, L., Zhu, S., Huang, D., An, J., Lou, S., Tao, S., Wang, Q., Yan,
 622 R., Ma, Y., Chen, C., Cheng, Y., Su, H., and Huang, C.: Long-term trends and drivers of aerosol
 623 pH in eastern China, *Atmos. Chem. Phys.*, 22, 13833–13844, [https://doi.org/10.5194/acp-22-](https://doi.org/10.5194/acp-22-13833-2022)
 624 [13833-2022](https://doi.org/10.5194/acp-22-13833-2022), 2022.

625 Zhou, W., Gao, M., He, Y., Wang, Q., Xie, C., Xu, W., Zhao, J., Du, W., Qiu, Y., Lei, L., Fu, P., Wang,
626 Z., Worsnop, D. R., Zhang, Q., and Sun, Y.: Response of aerosol chemistry to clean air action in
627 Beijing, China: Insights from two-year ACSM measurements and model simulations, *Environ*
628 *Pollut.*, 255, 113345, <https://doi.org/10.1016/j.envpol.2019.113345>, 2019.

629 Zuend, A. and Seinfeld, J. H.: Modeling the gas-particle partitioning of secondary organic aerosol: the
630 importance of liquid-liquid phase separation, *Atmos. Chem. Phys.*, 12, 3857–3882,
631 <https://doi.org/10.5194/acp-12-3857-2012>, 2012.

632 Zuend, A., Marcolli, C., Peter, T., and Seinfeld, J. H.: Computation of liquid-liquid equilibria and phase
633 stabilities: implications for RH-dependent gas/particle partitioning of organic-inorganic aerosols,
634 *Atmos. Chem. Phys.*, 10, 7795–7820, <https://doi.org/10.5194/acp-10-7795-2010>, 2010.

635



637
638 **Figure 2. Long-term trends in the concentrations of $PM_{2.5}$ and its chemical components in from 2011**
639 **to 2022 in Zhengzhou. Box plots depict annual averages (red dots) and medians (black lines), the top,**
640 **middle, and bottom lines represent the 75, 50, and 25 percentiles of statistical data, respectively, and**
641 **the upper and lower whiskers represent the 90 and 10 percentiles of statistical data, respectively.**

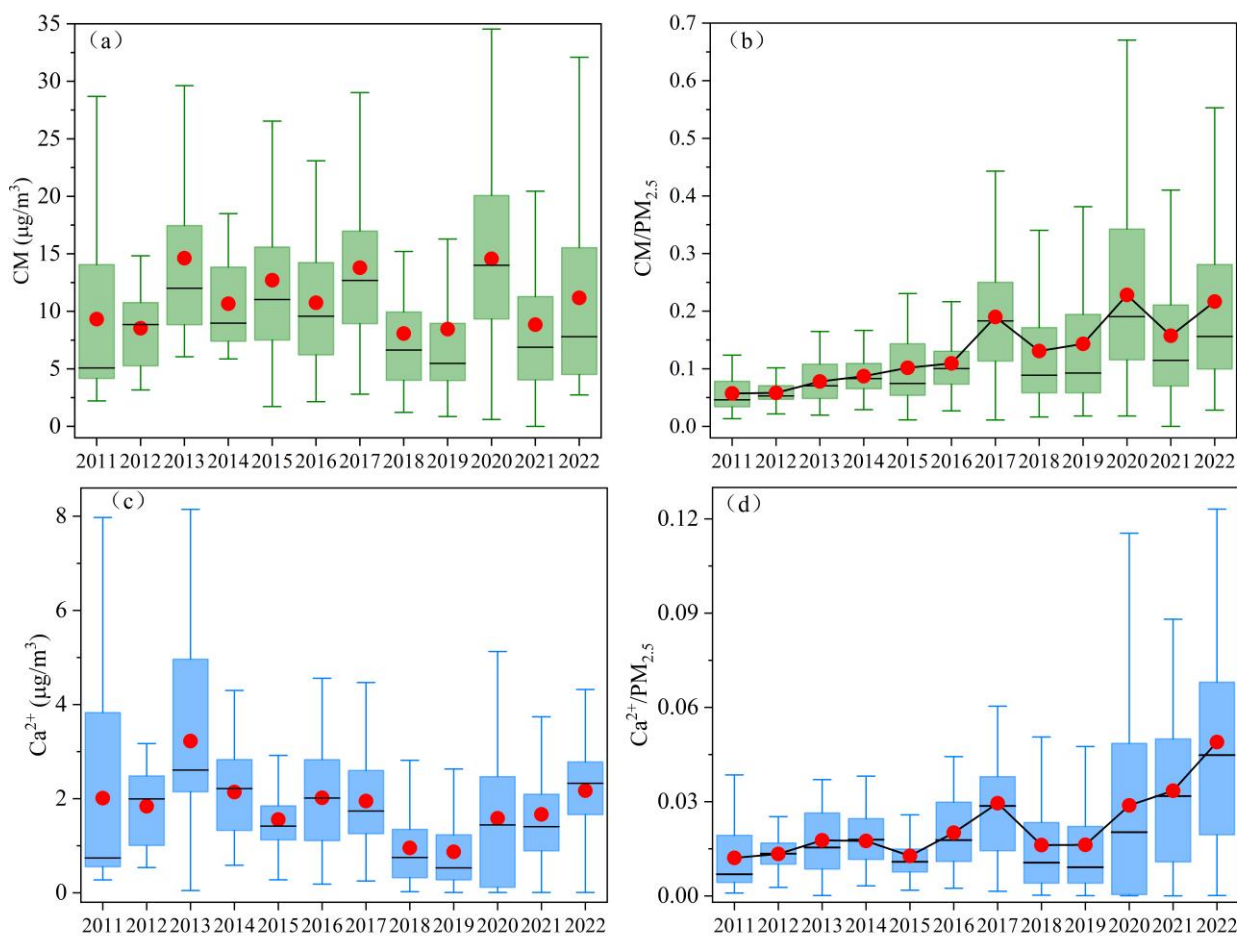


Figure 3. (a) and (c) Long-term trends in CM and Ca²⁺ concentrations in Zhengzhou from 2011 to 2022, respectively. Box plots depict annual averages (red dots) and medians (black lines). (b) and (d) Long-term trends in the proportions of CM and Ca²⁺ in PM_{2.5}, respectively.

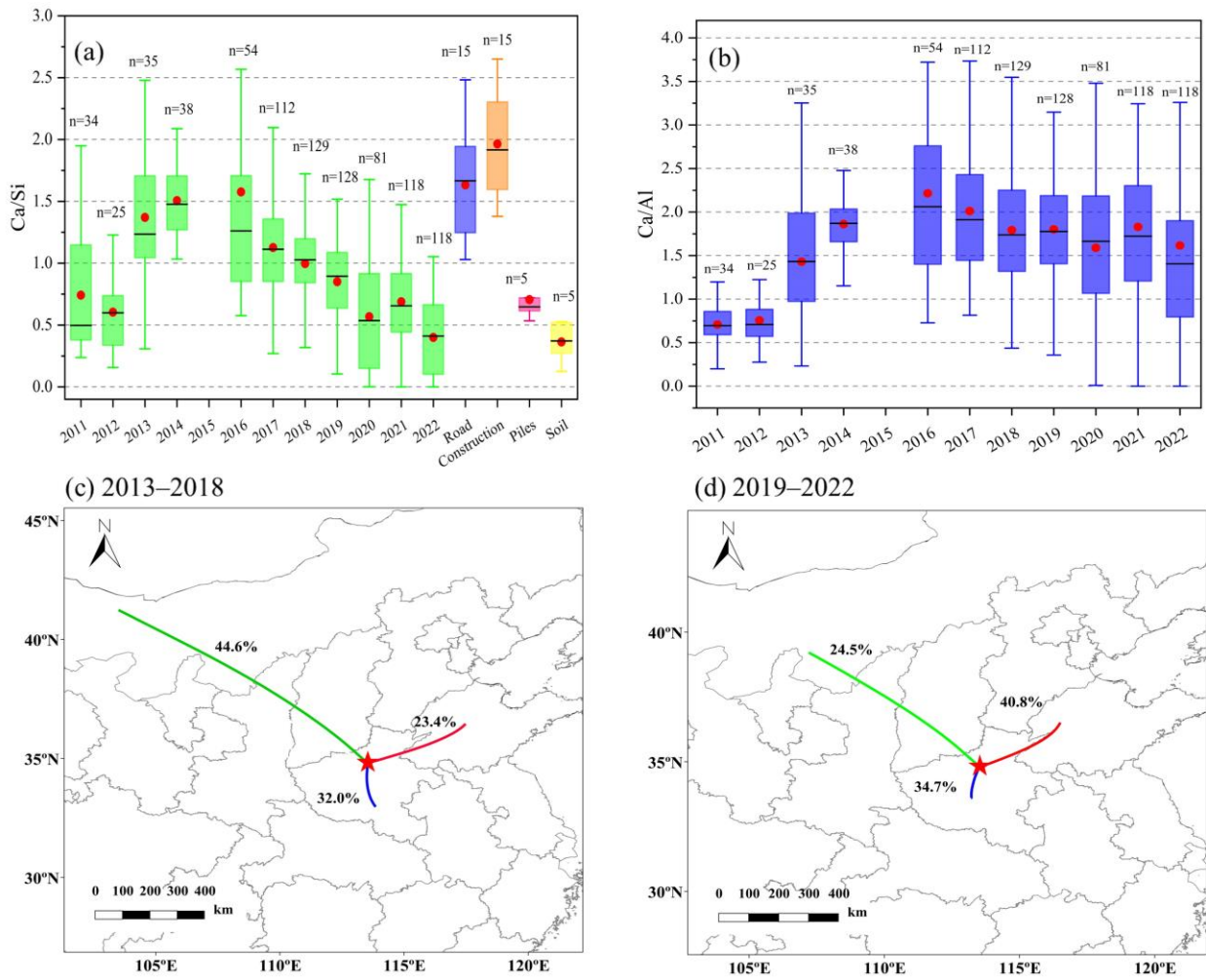


Figure 4. (a) The annual Ca/Si ratios in Zhengzhou from 2011 to 2022 compared with those in various dust sources (specific values and references in Table S5). The red dots and black lines in the box plots represent the annual averages and medians, respectively, with n indicating the sample size. (b) The Ca/Al ratios in Zhengzhou from 2011 to 2022. The red dots and black lines in the box plots represent the annual averages and medians, respectively, with n indicating the sample size. (c) and (d) The transport pathways of CM during 2013–2018 and 2019–2022, respectively.

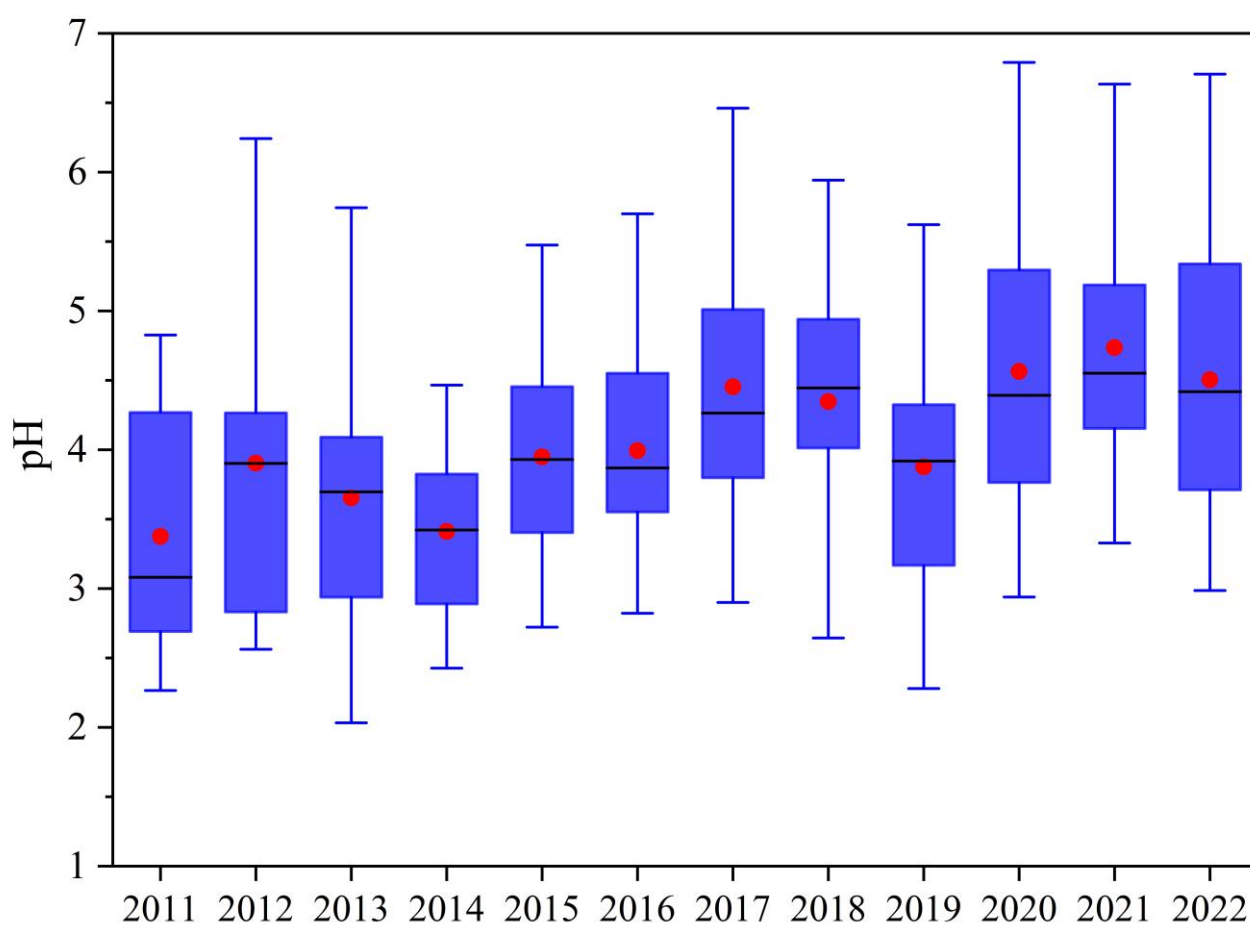


Figure 5. The time series of particle pH in Zhengzhou from 2011 to 2022. In the boxplots, red dots and black lines represent the annual mean and median values, respectively.

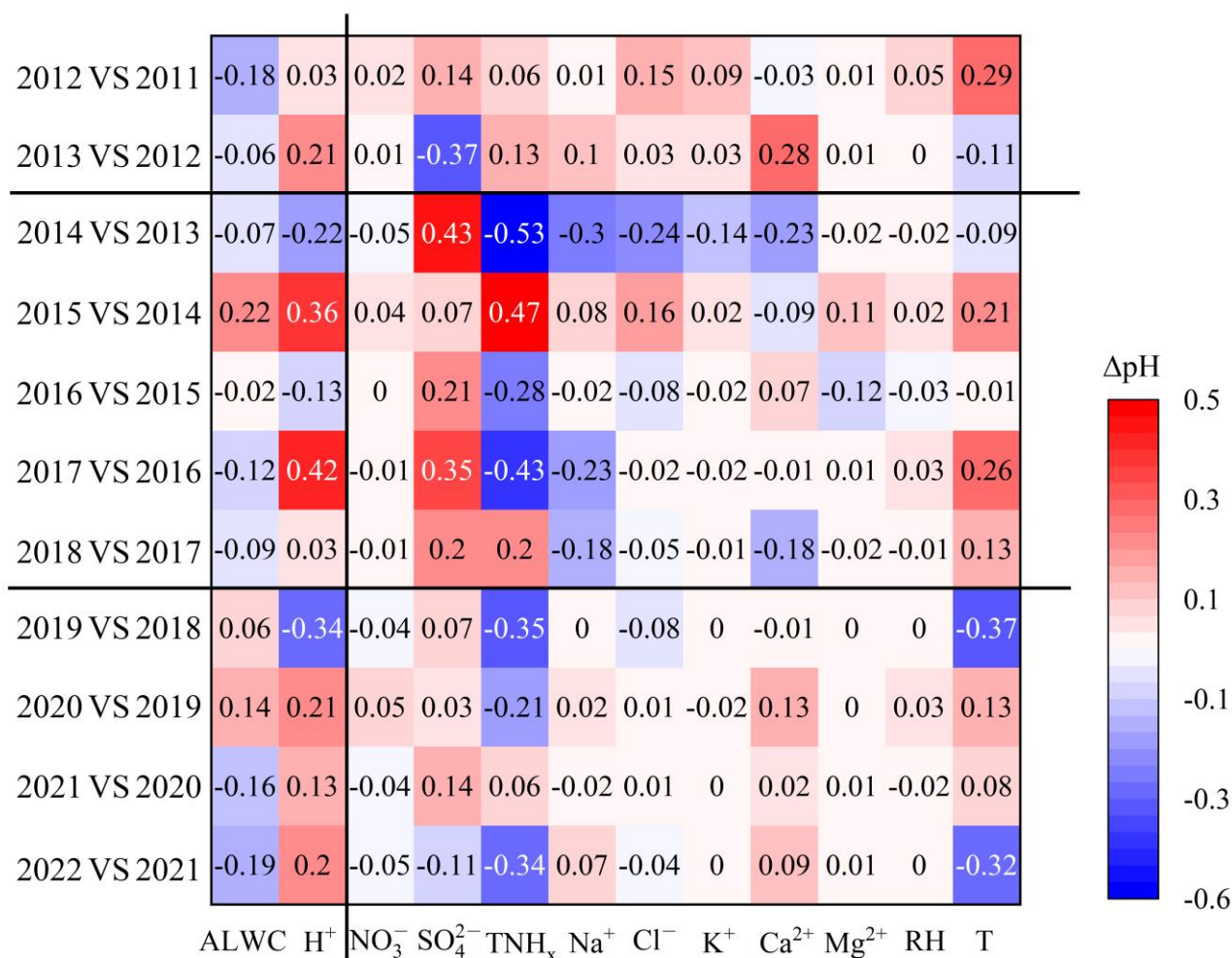


Figure 6. Contribution of each component to the changes in pH (ΔpH) between adjacent years. The difference between component concentrations and meteorological parameters between adjacent years is listed in Table S6.

660 **Table**661 **Table 1. Annual average concentrations of PM_{2.5} and its components from 2011 to 2022 in Zhengzhou, China (μg/m³).**

Years	PM _{2.5}	EC	OC	NO ₃ ⁻	SO ₄ ²⁻	NH ₄ ⁺	CM	Ca ²⁺
2011	161.9 ± 81.4	5.1 ± 2.1	13.6 ± 8.6	16.2 ± 11.2	29.6 ± 14.3	13.8 ± 8.3	9.3 ± 7.3	2.0 ± 2.2
2012	157.9 ± 71.2	5.6 ± 2.5	20.0 ± 13.4	20.2 ± 13.7	25.0 ± 11.2	15.0 ± 7.1	8.5 ± 3.4	1.8 ± 0.8
2013	212.4 ± 101.5	6.9 ± 3.8	21.5 ± 10.4	22.7 ± 13.2	38.0 ± 19.9	17.1 ± 6.9	14.6 ± 8.3	3.2 ± 2.1
2014	130.8 ± 48.7	4.6 ± 2.0	14.2 ± 8.2	15.5 ± 10.8	23.4 ± 9.3	10.2 ± 6.2	10.7 ± 4.4	2.1 ± 1.0
2015	146.1 ± 61.0	10.0 ± 4.7	23.2 ± 11.6	20.6 ± 14.5	21.6 ± 9.8	15.7 ± 7.5	12.7 ± 6.8	1.6 ± 0.7
2016	117.4 ± 73.5	4.0 ± 2.8	14.4 ± 10.0	20.4 ± 18.7	17.1 ± 11.3	11.9 ± 10.6	10.8 ± 5.3	2.0 ± 1.1
2017	91.5 ± 61.1	3.1 ± 2.5	13.7 ± 7.5	17.6 ± 15.9	11.8 ± 11.6	8.4 ± 7.9	13.8 ± 6.5	2.0 ± 1.0
2018	76.8 ± 41.6	1.5 ± 0.7	13.4 ± 7.3	16.7 ± 13.5	9.4 ± 6.0	9.7 ± 6.1	8.1 ± 5.7	1.0 ± 0.8
2019	68.4 ± 34.8	1.5 ± 0.8	11.5 ± 6.8	13.8 ± 13.9	8.6 ± 6.4	7.5 ± 6.1	8.5 ± 7.8	0.9 ± 0.9
2020	75.5 ± 31.8	2.1 ± 0.9	13.3 ± 7.9	18.6 ± 14.2	8.3 ± 5.6	6.7 ± 6.6	14.6 ± 7.6	1.6 ± 1.4
2021	71.5 ± 45.9	1.7 ± 0.9	13.0 ± 8.0	15.1 ± 15.1	6.1 ± 4.5	6.8 ± 6.0	8.9 ± 7.0	1.7 ± 1.2
2022	59.5 ± 41.1	1.6 ± 1.5	9.1 ± 8.1	10.0 ± 14.4	7.9 ± 4.5	5.5 ± 5.4	11.2 ± 8.3	2.2 ± 1.1

662

663 Supplement materials:

664 Text S1 Instruments and Measurements.

665 Samples were collected using a high-volume sampler (TE-6070D, Tisch, USA) and air particulate
666 samplers (TH-16A, Tianhong, China) from April 2011 to December 2022. Two quartz filters and two
667 Teflon filters were used daily from 10:00 AM to 9:00 AM the next day, resulting in a total of 5848
668 samples. After excluding abnormal data due to instrument malfunctions, 4228 valid samples were
669 obtained. Detailed information on the samples is provided in Table S1.

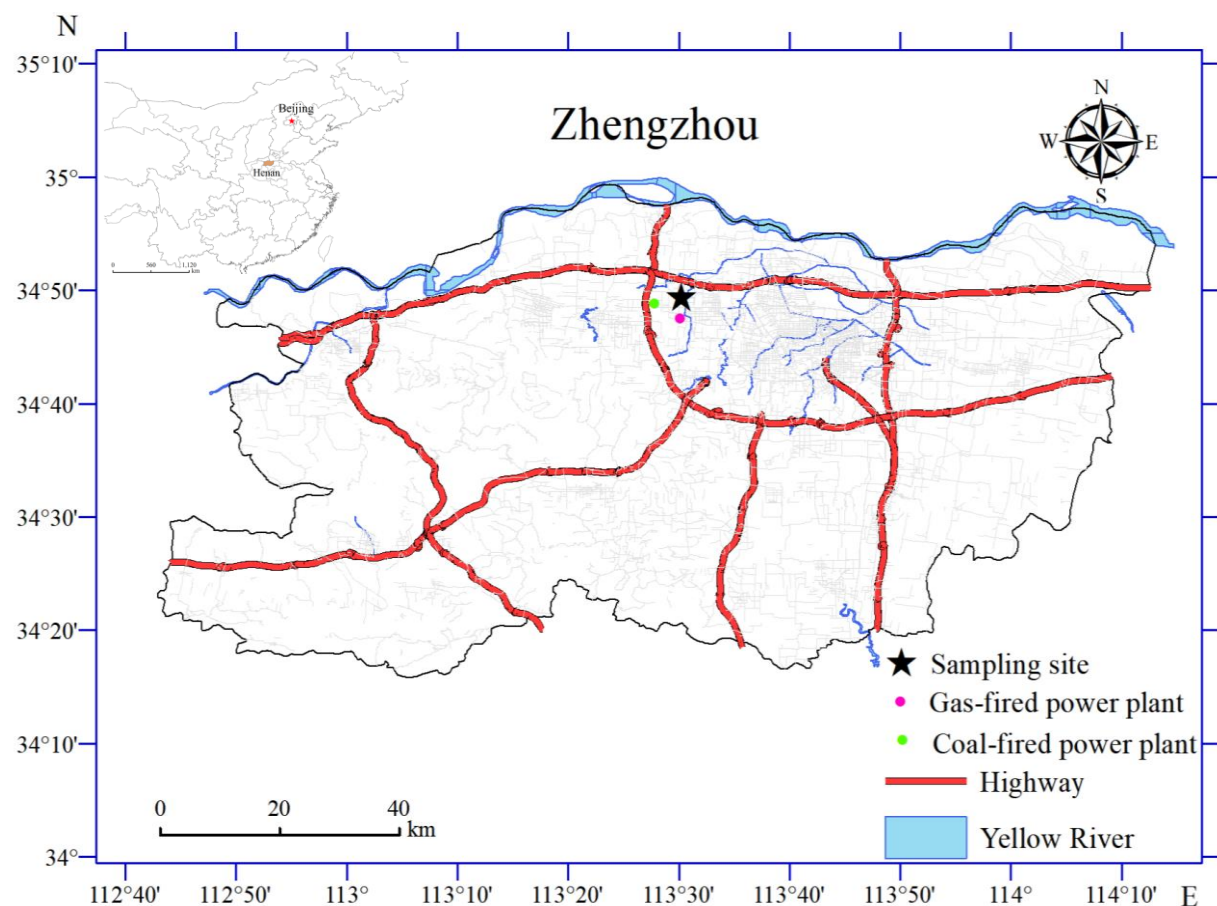
670 Organic carbon (OC) and elemental carbon (EC) were analyzed using a carbon analyzer (Model
671 5L, Sunset Laboratory, USA). The analysis of EC and OC was conducted in two stages. In the first
672 stage, the filter membrane was placed in a quartz heating furnace under a pure helium atmosphere. As
673 the temperature gradually increased to approximately 580°C, OC was volatilized and released. In the
674 second stage, heating continued in a mixed atmosphere of 2% oxygen and 98% helium. When the
675 temperature reached approximately 870°C, EC underwent oxidative decomposition and was released.
676 During the helium flow transmission, OC and EC released at different temperatures were completely
677 oxidized to CO₂ in a MnO₂ oxidation furnace and subsequently reduced to CH₄ for detection by a flame
678 ionization detector (FID). The detection limits for both OC and EC were 0.2 µg/cm². Before each
679 sample analysis, calibration was performed using a standard sucrose solution. Additionally, parallel
680 tests were conducted every ten samples to ensure accuracy.

681 Water-soluble inorganic ions (Cl⁻, NO₃⁻, SO₄²⁻, Na⁺, NH₄⁺, K⁺, Mg²⁺, and Ca²⁺) were measured
682 using ion chromatography (ICS-90 and ICS-900 models, Dionex, USA). Half of the PM_{2.5} filter was

683 cut into pieces and ultrasonically extracted with 20 mL of Milli-Q water for 30 min, followed by
684 filtering through a 0.45 mm polytetrafluoroethylene syringe filter before analysis. The cation
685 concentrations were determined by an IonPacASII-HC4 mm anion separation column and an
686 IonPacAGII-HC4 mm guard column, with 20 mM methane sulfonate as an eluent at 0.8 mL/min. The
687 anions were measured by an IonPacCS12A cation separation column and an IonPacCG12A guard
688 column, with a solution of 8.0 mM Na₂CO₃ + 1.0 mM NaHCO₃ as an eluent at 1.0 mL/min. The
689 regression coefficients (R^2) of the calibration curves were over 0.9996 for all ions, except NH₄⁺
690 (0.9988), which showed a quadratic response.

691 Elements were analyzed using a wavelength dispersive X-ray fluorescence spectrometer (S8
692 TIGER, Bruker, Germany) to determine concentrations of Fe, Na, Mg, Al, Si, Cl, K, Ca, V, Ni, Cu, Zn,
693 Cr, Mn, Co, Cd, Ga, As, Se, Sr, Sn, Sb, Ba, and Pb (Tremper et al., 2018), which has been approved
694 by the United States Environmental Protection Agency (Chow and Watson, 1994). The spectrometer
695 was equipped with an X-ray tube featuring close coupling among the tube, sample, and detector,
696 ensuring high efficiency and optimal excitation of elements within the sample. Before analysis, the
697 instrument was calibrated using a series of high-quality, self-prepared standards. Calibration
698 procedures were conducted following established methods (Chow and Watson, 1994). To assess
699 potential contamination and ensure data quality, blank filters were routinely analyzed alongside each
700 batch of samples.

701



703
704 **Figure S1. Sampling site in Zhengzhou, China. © 2019 National Geomatics Center of China. All**
705 **rights reserved.**
706

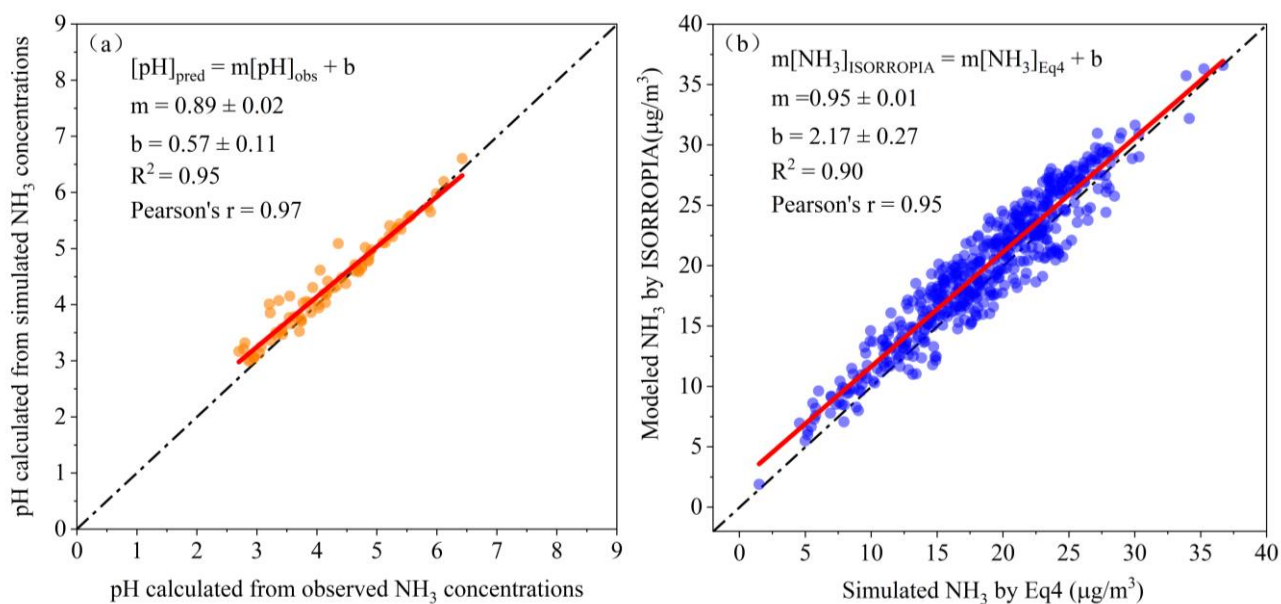


Figure S2. Verification of the NH₃ Method.

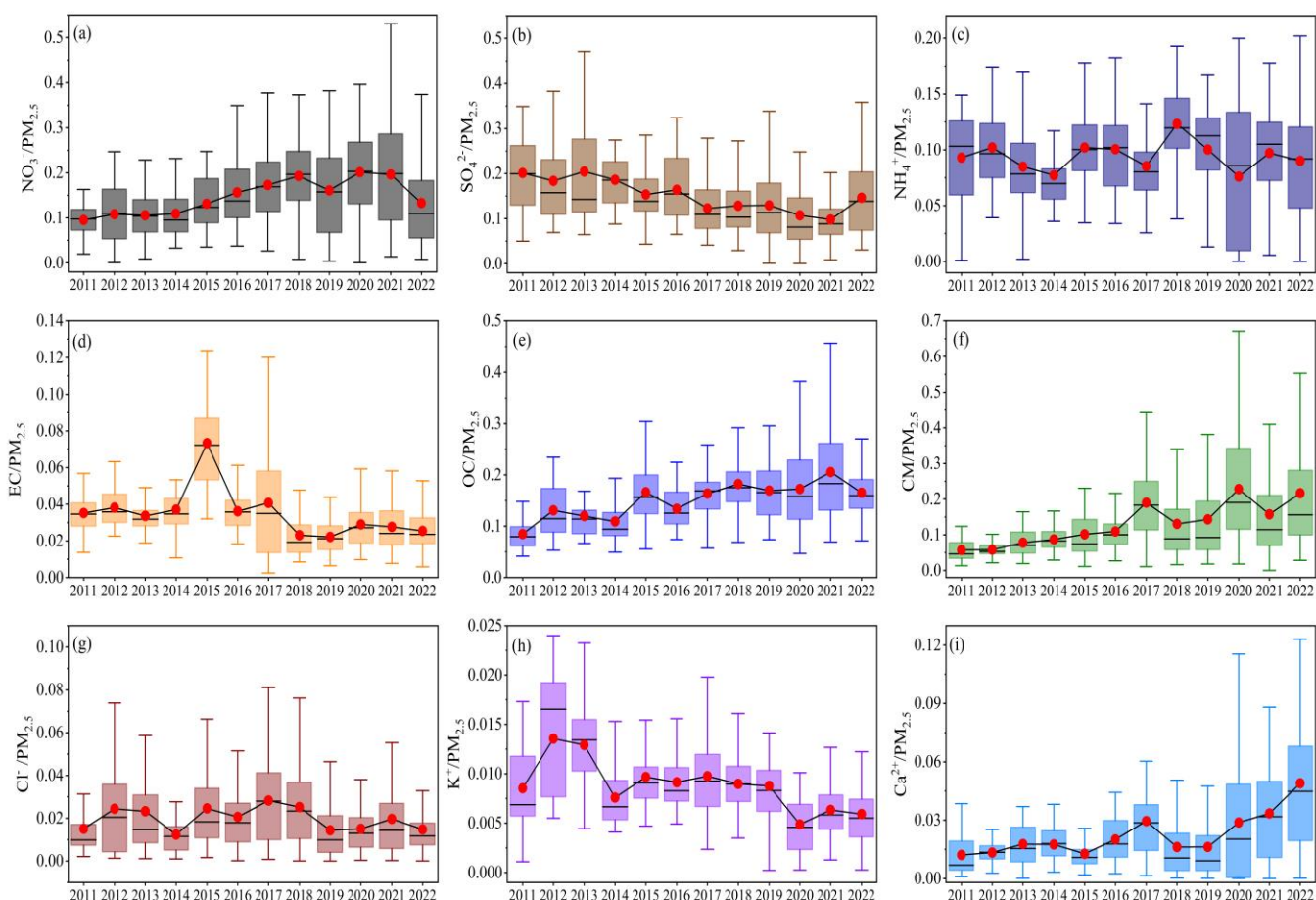


Figure S3. Trends in the proportions of chemical components in PM_{2.5} from 2011 to 2022.

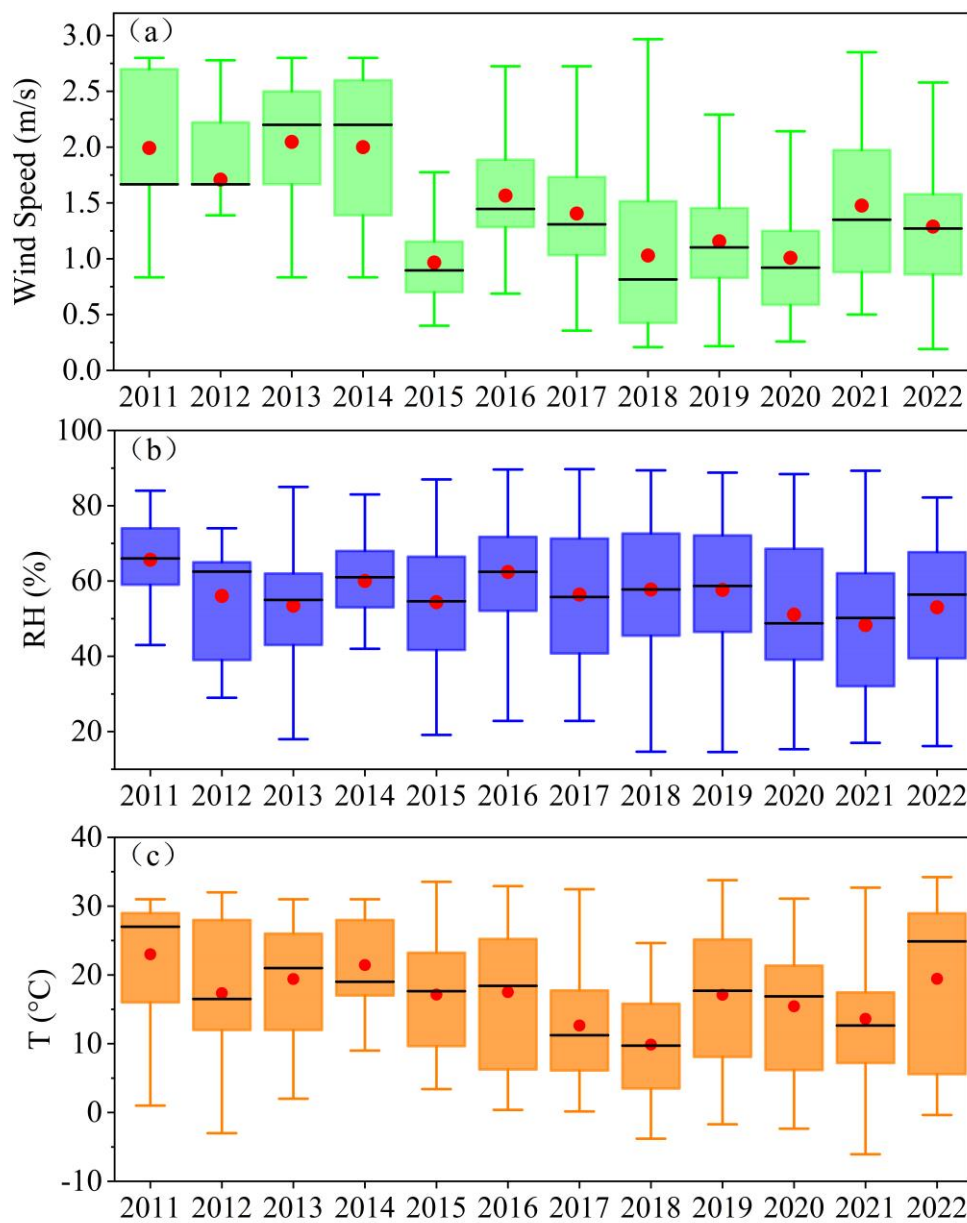


Figure S4. Trends in the meteorological parameters from 2011 to 2022.

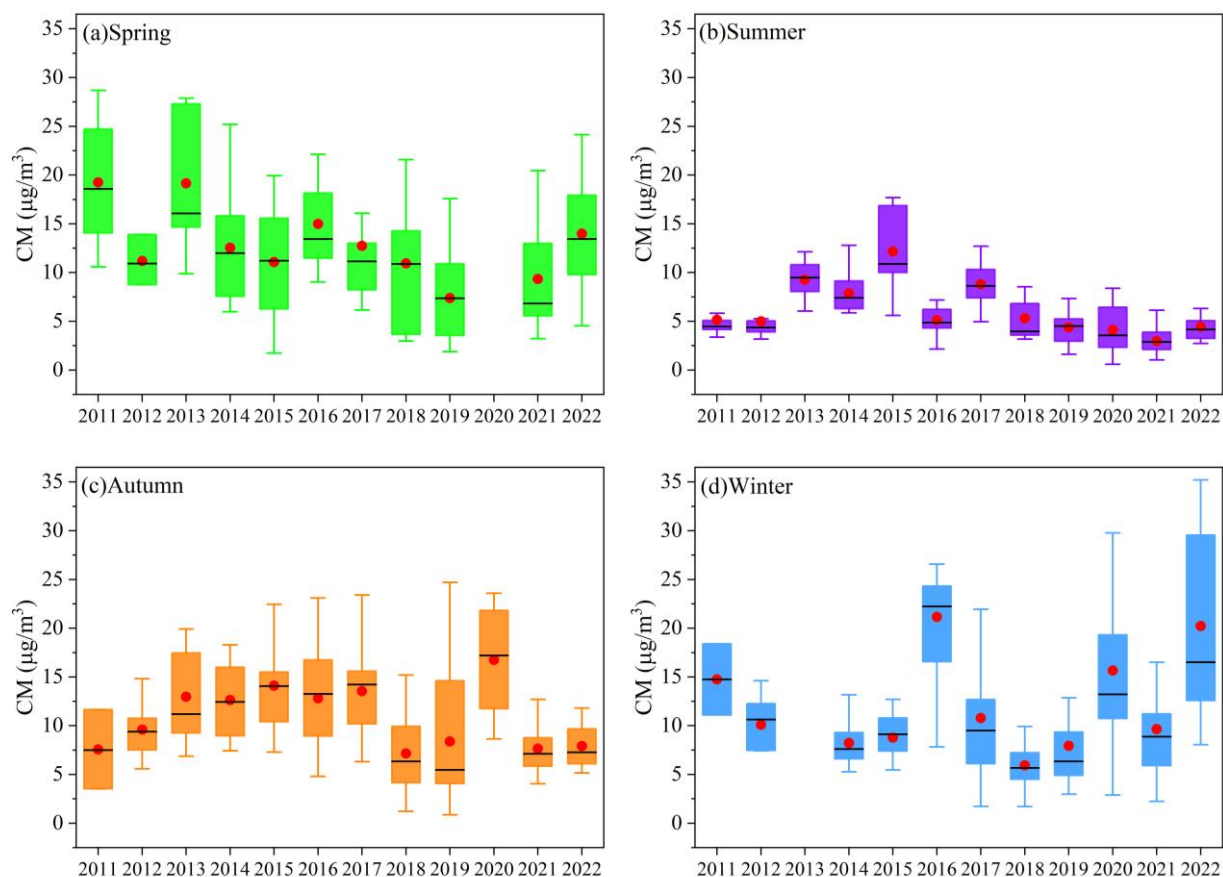


Figure S5. Trends in the CM concentrations in different seasons from 2011 to 2022.

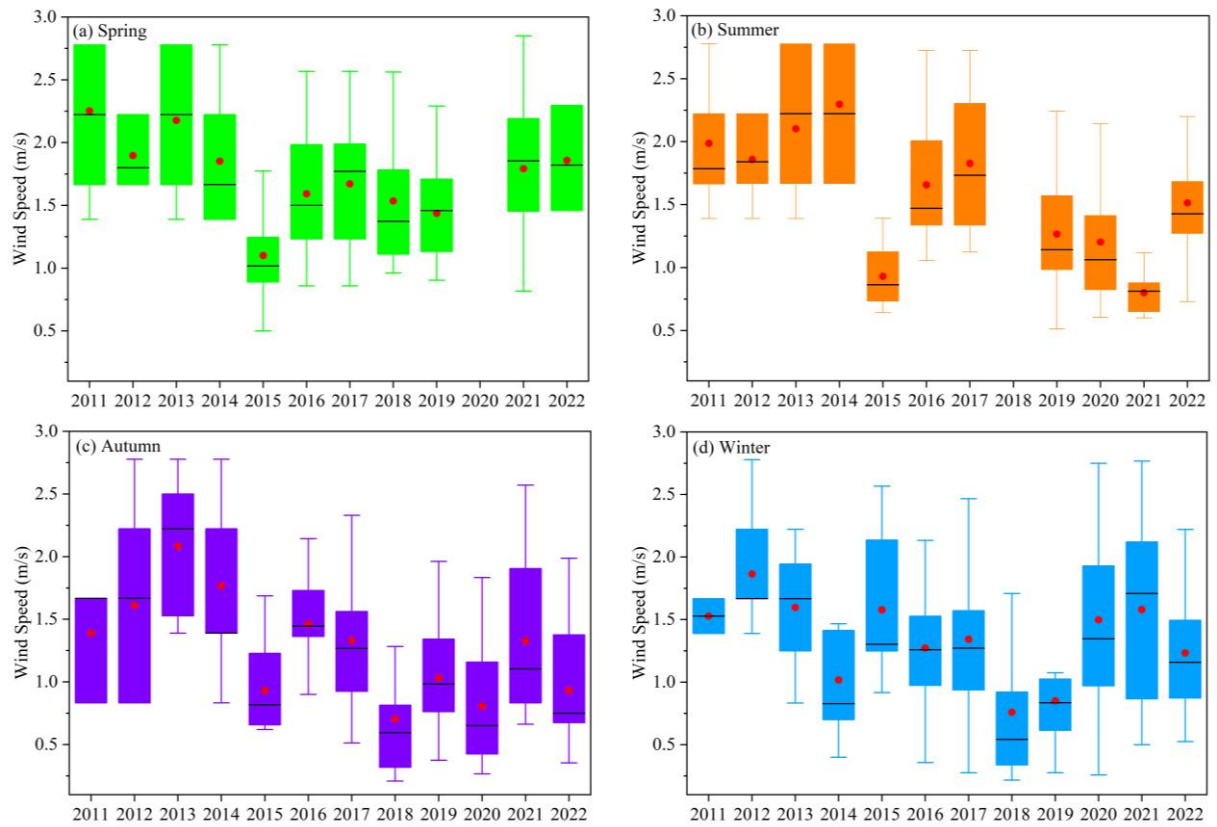


Figure S6. The variation in WS across different seasons from 2011 to 2022.

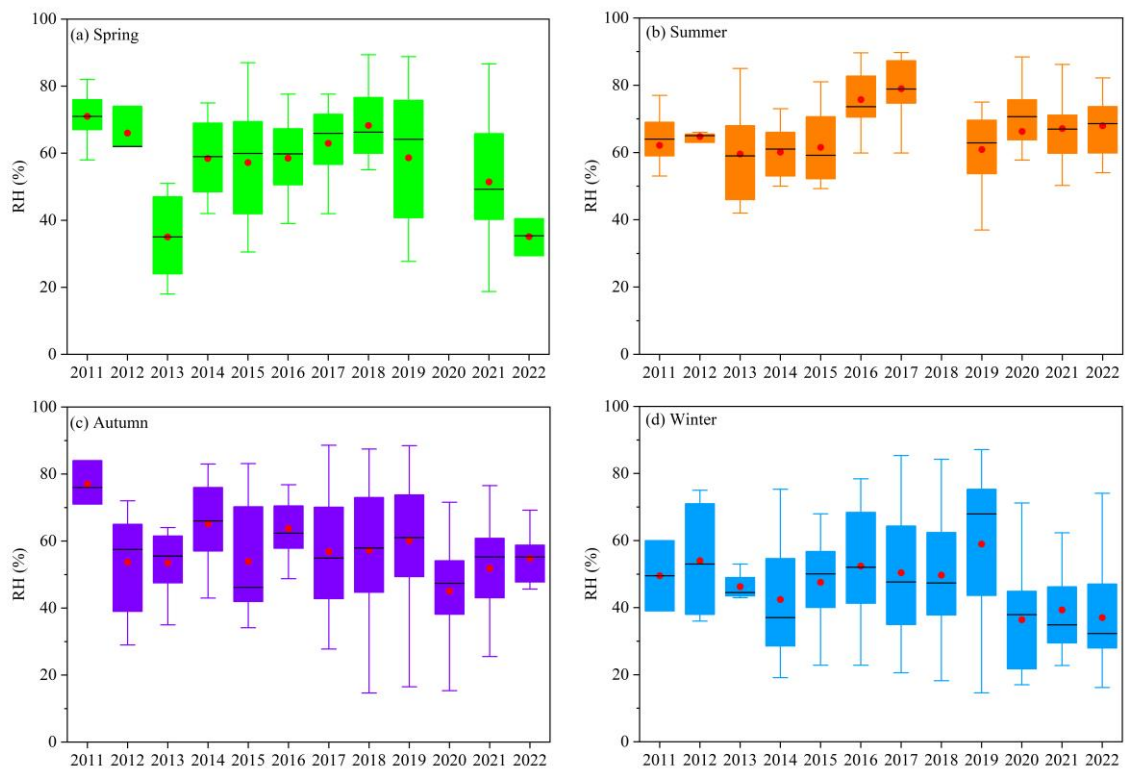


Figure S7. The variation in RH across different seasons from 2011 to 2022.

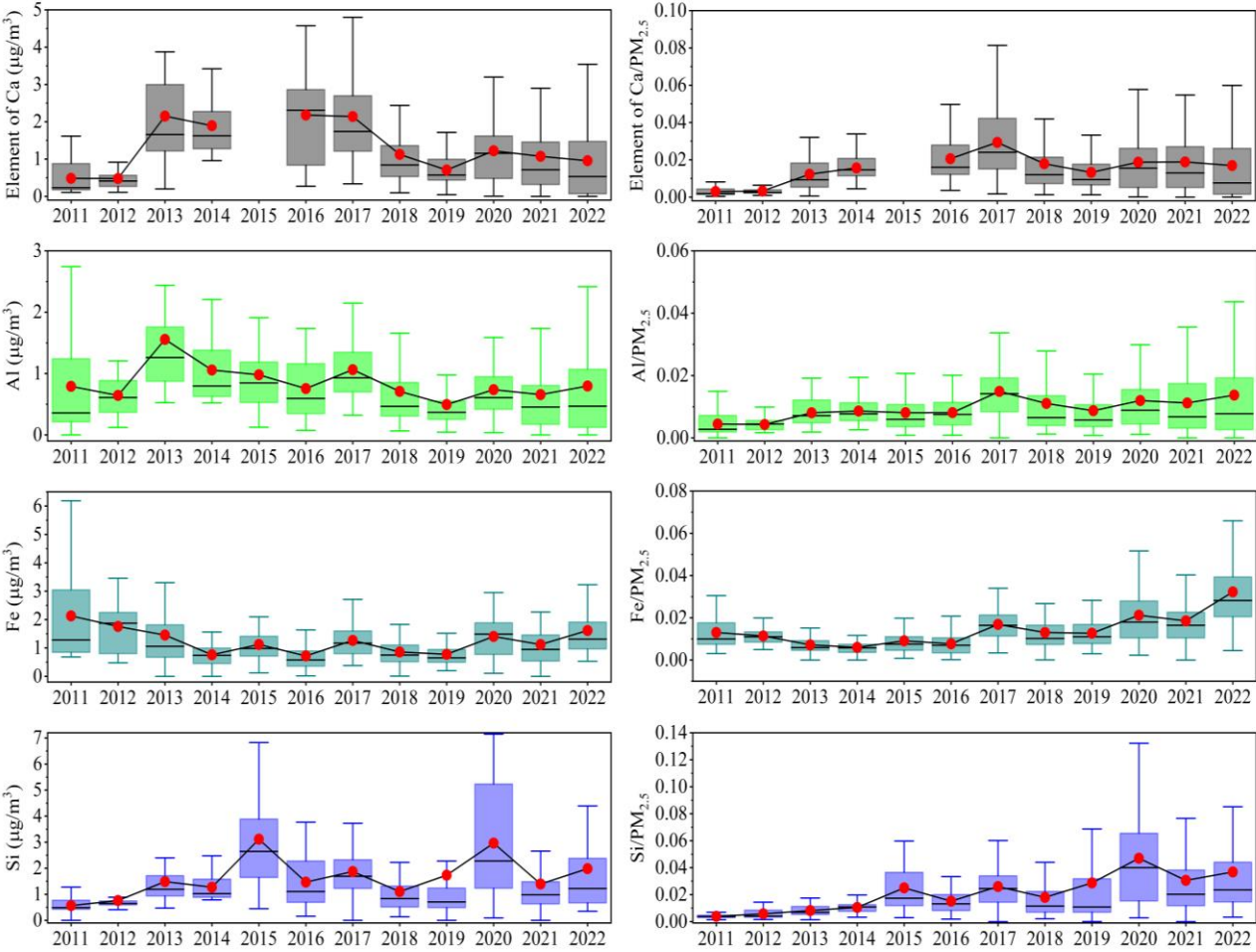


Figure S8. Trends in the concentrations of crustal elements and their proportions in $\text{PM}_{2.5}$ from 2011 to 2022.

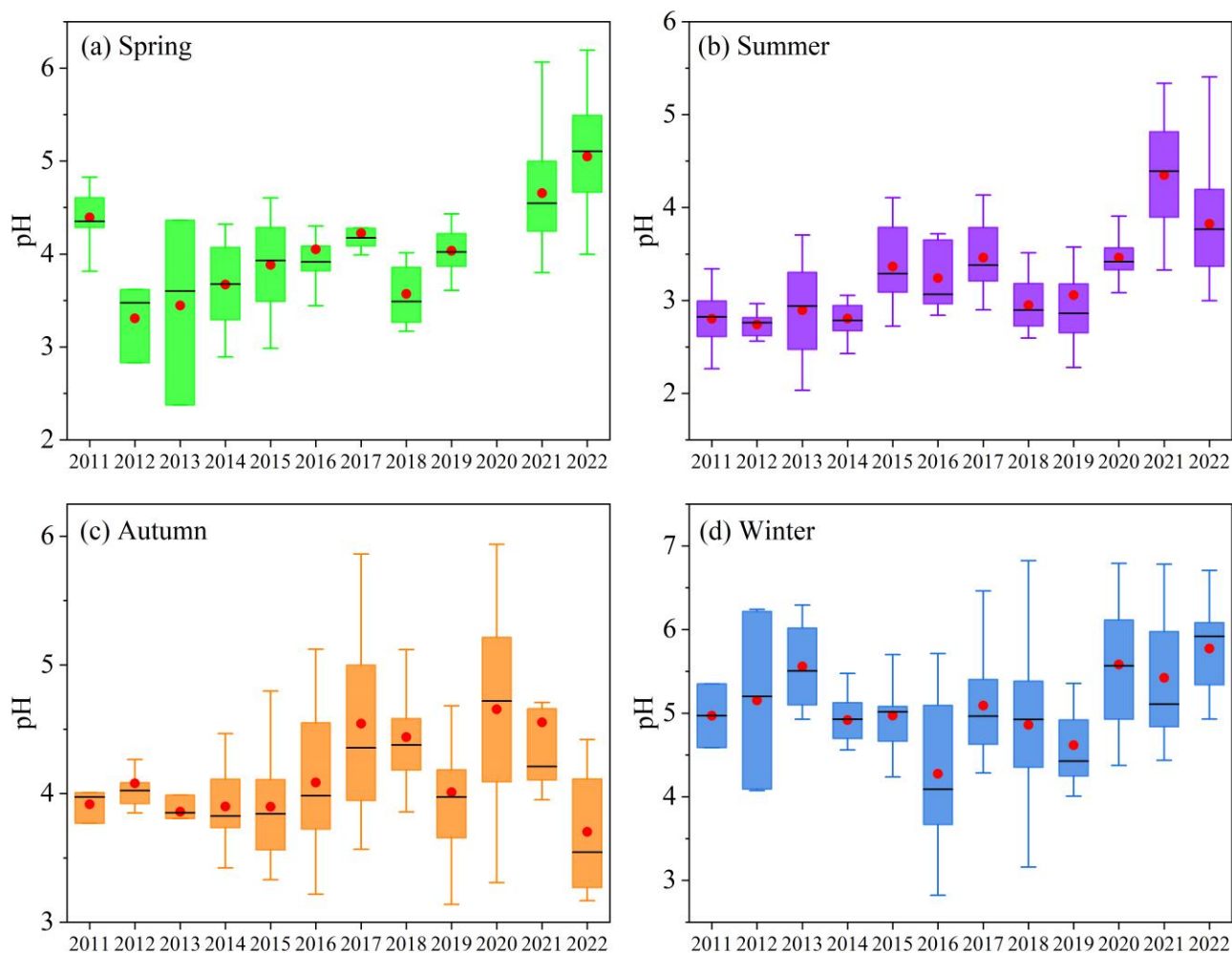


Figure S4. Trends in the particle pH in different seasons from 2011 to 2022.

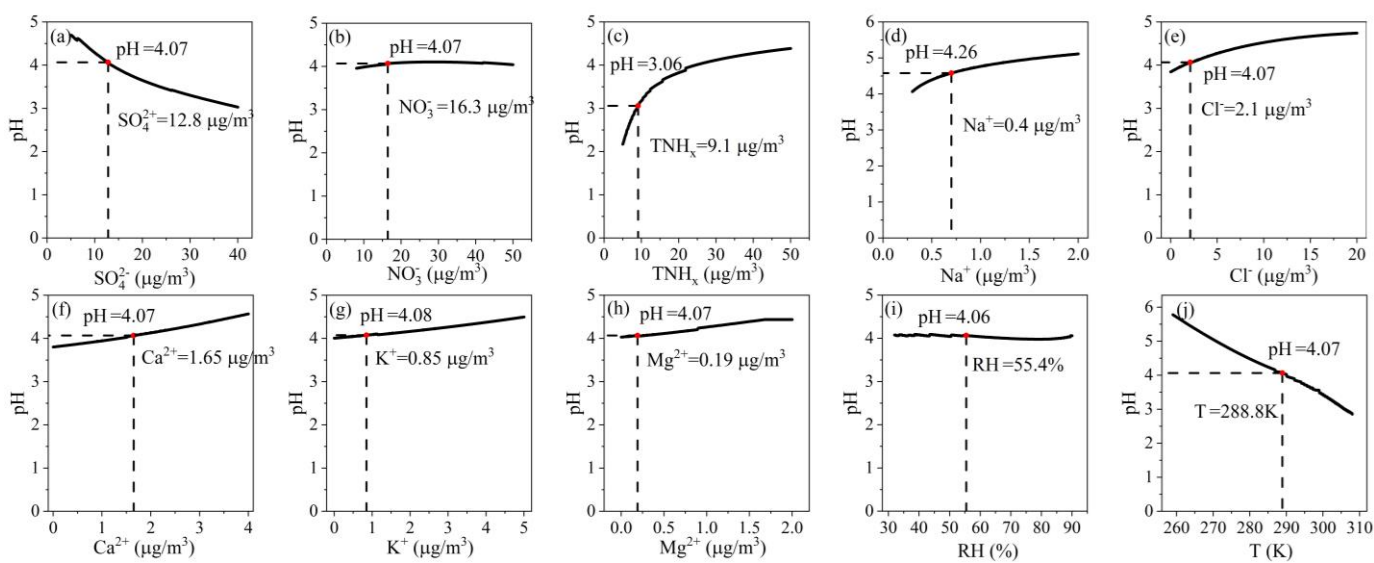


Figure S5. Sensitivity analysis of input parameters to particle pH. The dashed line represents the average of the observational data from 2011 to 2022.

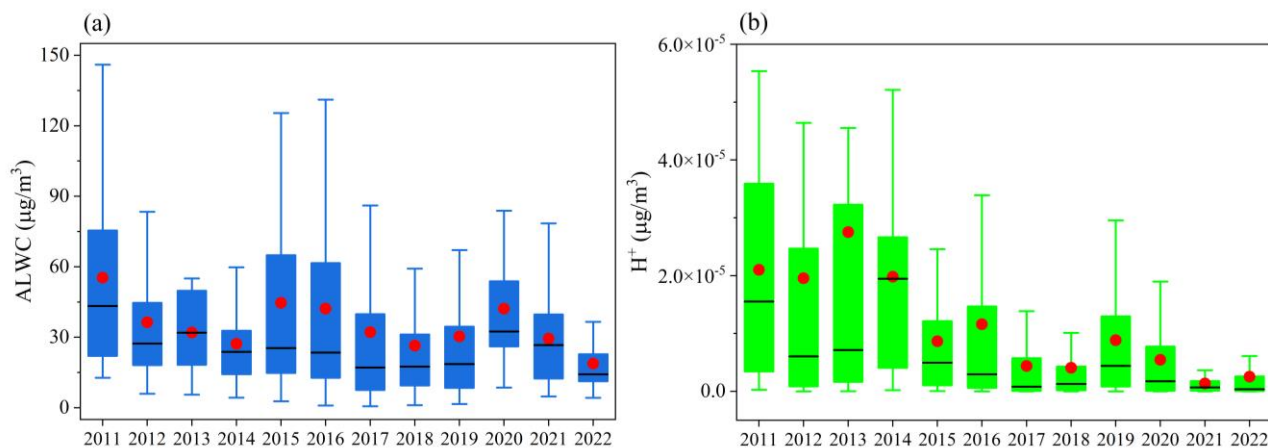


Figure S6. Trends in aerosol liquid water content (ALWC) and H^+ concentrations from 2011 to 2022

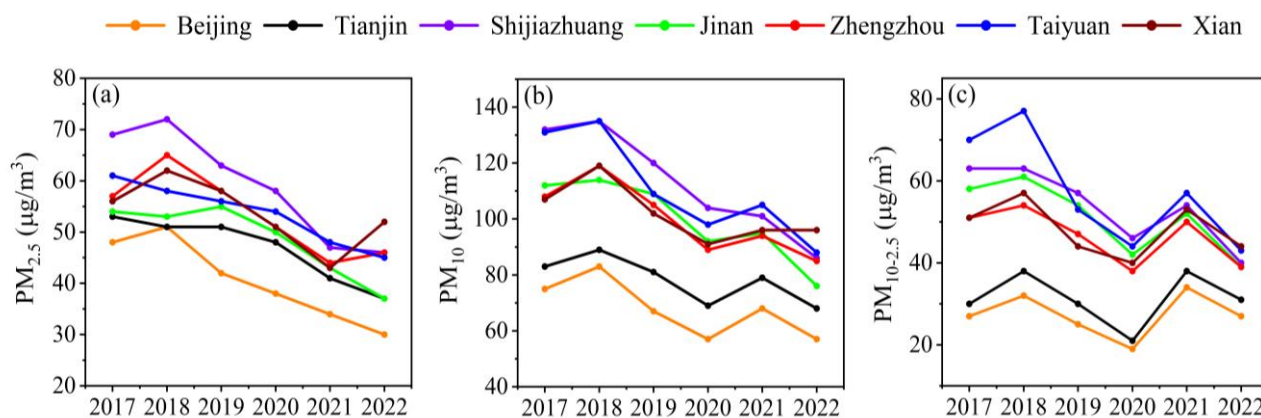


Figure S7. Trends in the annual average concentrations of $\text{PM}_{2.5}$, PM_{10} , and $\text{PM}_{10-2.5}$ in provincial capitals in the North China Plain.

747 Table S1. Information on sampling date and numbers.

Years	Sampling date	The effective number of samples
2011	April 7–20 July 1–31 October 28–December 2 December 11–November 23	188
2012	February 25–26 April 21–May 6 July 22–August 2 October 17–November 1 December 8–25	140
2013	February 25–March 6 April 1–May 1 June 5–July 30 September 20–October 13 December 2–18	184
2014	April 1–May 5 June 18–July 20 October 7–24 December 30–31	180
2015	January 1–15 April 1–20 July 1–20 October 9–24	248
2016	January 6–22 April 8–30 July 9–31 October 1–20 December 29–31	252
2017	January 1–20 April 18–May 4 July 1–26 October 14–December 31	480
2018	January 1–31 April 1–30 July 1–31 October 9–December 31	600
2019	January 1–31 April 1–30 July 1–31 September 2–October 31 November 12–30 December 21–31	592

2020	January 1–20 June 5–July 31 October 6–November 13 December 15–31	332
2021	January 1–31 March 16–April 30 July 1–August 8 October 17–December 31	540
2022	January 1–4 April 1–May 3 July 1–August 11 September 5–October 11 December 10–31	492
Total		4228

Table S2. The method detection limit (MDL) and measurement uncertainties (Unc) of individual components

	MDLs ($\mu\text{g}/\text{m}^3$)	Unc (%)
EC	0.1	13.1
OC	0.1	9.8
Na ⁺	0.005	9.6
NH ₄ ⁺	0.011	10.1
K ⁺	0.006	9.5
Mg ²⁺	0.002	9.3
Ca ²⁺	0.017	8.8
F ⁻	0.001	8.2
Cl ⁻	0.001	9.3
NO ₃ ⁻	0.015	10.1
SO ₄ ²⁻	0.031	9.9
Na	0.003	10.9
Mg	0.002	10.6
Al	0.004	9.2
Si	0.005	9.3
Cl	0.008	9.5
K	0.005	9.4
Ca	0.01	9.4
V	0.008	57.9
Ni	0.006	96.6
Cr	0.02	24.7
Mn	0.02	16.8
Fe	0.03	9.3
Co	0.009	79.6
Cu	0.005	5.8
Zn	0.003	8.4
Ga	0.005	84.7
As	0.008	27.4

Se	0.006	25.7
Sr	0.006	22.8
Cd	0.03	68.6
Sn	0.02	42.0
Sb	0.02	73.6
Ba	0.02	15.6
Pb	0.02	13.4

Table S3. Control measures for dust implemented by Henan Province and Zhengzhou government

Release time	Policies	Regulatory focus
2013.9	Regulations on Reducing Pollutant Emissions in Henan Province	Road, Construction
2014.8	Temporary Regulations on Dust Control Management at Construction Sites in Henan Province	Construction
2016.7	Implementation Plan for Controlling Dust Pollution in Henan Province	Road, Construction
2018.2	Regulations on the Prevention and Control of Atmospheric Pollution in Henan Province	Road, Construction, Piles
2019.4	Special Action Plan for Fine Management of Dust Pollution Prevention and Control at Construction Sites in Zhengzhou City, 2019	Construction
2019.8	Enhanced Action Plan for Intensive Dust Control at Construction Sites in 2019	Construction
2021.1	Special Governance Plan for Key Project Dust Pollution in Zhengzhou	Road, Construction, Piles

759

Table S4. Analysis of the inter - annual trends of CM and Ca²⁺ concentrations and pH during different periods using multiple methods.

	2011–2013			2013–2019			2019–2022		
	CM	Ca ²⁺	pH	CM	Ca ²⁺	pH	CM	Ca ²⁺	pH
MK-Z	3.01	2.70	1.41	-9.74	-13.62	3.00	2.48	8.21	5.12
MK- <i>p</i>	0.003	0.007	0.159	<2.2 E-16	<2.2E-16	0.003	0.013	2.20E-16	2.99E-07
Sen's slope	0.082	0.023	7.10E-03	-0.015	-4.14E-03	9.15E-04	5.80E-03	5.42E-03	2.93E-03
LS slope	2.65	0.61	/	-0.81	-0.32	0.11	0.24	0.40	0.21

760

** MK-Z and MK-*p* represent the trend (Z) and significance (*p*) calculated by the Mann - Kendall method using daily data, respectively; Sen's

761

slope represents the Sen slope using daily data; LS slope represents the Least - Squares slope using annual data. All the above calculations were

762

performed using the R language (R version 4.0.2).

763

Table S5. The ratios of Ca/Si in the source spectrum of different dust sources in China

Dust source	City	Ca/Si	Reference
Road dust	Xi'an	2.04	http://www.klap.ac.cn/wgPMzypfypk/ycy/201706/t20170610_375562.html
	Yinchuan	2.48	
	Lanzhou	1.67	
	Beijing	1.25	
	Tianjin	1.03	
	Baoding	1.16	
	Shijiazhuang	1.98	
	Handan	1.83	
	Shenyang	1.81	
	Changsha	1.92	
	Chongqing	1.38	
	Chengdu	1.17	
	Kunming	1.94	
	Taiyuan	1.55	
	Nanjing	1.28	
Construction dust	Xi'an	1.69	http://www.klap.ac.cn/wgPMzypfypk/ycy/201706/t20170610_375562.html
	Yinchuan	1.84	
	Lanzhou	2.33	
	Beijing	2.65	
	Tianjin	1.46	
	Baoding	1.58	
	Shijiazhuang	1.38	
	Handan	1.86	
	Shenyang	1.92	
	Changsha	2.30	
	Chongqing	2.52	
	Chengdu	2.15	
	Kunming	1.60	
	Taiyuan	1.92	
	Nanjing	2.26	
Piles dust	Xi'an	0.72	(Yang, 2016)
	Tianjin	0.57	(Zhang et al., 2018)
	Taiyuan	0.61	(Bi et al., 2007)
	Jinan	1.01	(Bi et al., 2007)
	/	0.65	http://www.nkspap.com:9091/Index.aspx
Soil dust	Nanchang	0.37	(Xu et al., 2019)
	Xi'an	0.27	(Yang, 2016)
	Jincheng	0.13	(Wang et al., 2016)
	Wuhan	0.52	(Gong and Luo, 2018)
	/	0.53	http://www.nkspap.com:9091/Index.aspx

766

Table S6. The difference between component concentrations ($\mu\text{g}/\text{m}^3$) and meteorological parameters between adjacent years.

Years	ALWC	$\text{H}^+(10^{-6})$	NO_3^-	SO_4^{2-}	TNH_x	Na^+	Cl^-	K^+	Ca^{2+}	Mg^{2+}	RH(%)	T (°C)
2012VS2011	-19.0	-1.5	4.0	-4.6	1.3	0.02	2.0	0.9	-0.2	0.04	-9.6	-5.7
2013VS2012	-4.6	-7.6	2.6	13.0	2.1	0.2	0.4	0.3	1.4	0.1	-2.6	2.1
2014VS2013	-4.5	7.9	-7.3	-14.6	-6.9	-0.4	-3.4	-1.6	-1.1	-0.2	6.6	2.0
2015VS2014	17.6	-11.2	5.2	-1.8	5.5	0.1	2.1	0.4	-0.6	0.6	-5.6	-4.2
2016VS2015	-2.3	3.0	-0.2	-4.5	-3.7	-0.03	-0.1	-0.4	0.5	-0.7	8.0	0.3
2017VS2016	-10.0	-7.2	-2.9	-5.3	-3.6	-0.2	-0.3	-0.2	-0.1	0.1	-6.0	-4.9
2018VS2017	-5.8	-0.3	-0.8	-2.4	1.3	-0.1	-0.8	-0.2	-0.1	-0.1	1.4	-2.8
2019VS2018	4.1	4.8	-3.0	-0.8	-2.2	-0.04	-0.7	-0.03	-0.1	-0.01	-0.1	7.3
2020VS2019	11.6	-3.4	4.9	-0.3	-0.9	0.1	0.1	-0.2	0.7	0.02	-6.6	-2.1
2021VS2020	-12.7	-1.5	-3.6	-2.3	0.2	-0.01	0.03	0.01	0.1	0.04	-2.8	-1.5
2022VS2021	-10.6	-1.5	-5.1	1.9	-1.4	0.03	-0.3	0.01	0.5	0.04	4.7	5.8

767

768

References

- Bi, X., Feng, Y., Wu, J., Wang, Y., and Zhu, T.: Source apportionment of PM₁₀ in six cities of northern China, *Atmospheric Environment*, 41, 903–912, <https://doi.org/10.1016/j.atmosenv.2006.09.033>, 2007.
- Chow, J.C., Watson, J.G., 1994. Guidelines for PM₁₀ sampling and analysis applicable to receptor modeling. Washington, DC: US Environmental Protection Agency, Office of Air Quality Planning and Standards, EPA-452/R-94-009.
- Gong, P. and Luo, Y.: Study on the characteristics of source profiles in Wuhan, *Journal of Nanjing University of Information Science & Technology*, 10, 579–589, <https://doi.org/10.13878/j.cnki.jnuist.2018.05.008>, 2018.
- Tremper, A.; Font, A.; Priestman, M.; Hamad, S.; Chung, T.; Pribadi, A.; Brown, R.; Goddard, S.; Grassineau, N.; Petterson, K.; Kelly, F.; Green, D.: Field and laboratory evaluation of a high time resolution x-ray fluorescence instrument for determining the elemental composition of ambient aerosols, *Atmos. Meas. Tech.*, 11, 3541–3557, <https://doi.org/10.5194/amt-11-3541-2018>, 2018.
- Wang, Y., Peng, L., Li, L., Wang, Y., Zhang, T., Liu, H., and Mu, L.: Chemical compositions and sources apportionment of re-suspended dust in Jincheng, *Environmental Science*, 37, 82–87, <https://doi.org/10.13227/j.hjlx.2016.01.012>, 2016.
- Xu, Y., Gong, X., and Zhang, W.: Construction and characteristic analysis of PM_{2.5} source profiles of typical emissions in Nanchang City, *Chemical Engineer*, 33, 41–43, <https://doi.org/10.16247/j.cnki.23-1171/tq.20190841>, 2019.
- Yang, Y.: The Chemical Compositions and Source Apportionment of Particulate matter of Open Sources in Xi'an, 42–43, <https://doi.org/10.27393/d.cnki.gxazu.2016.000073>, 2016.
- Zhang, J., Wei, E., Wu, L., Fang, X., Li, F., Yang, Z., Wang, T., and Mao, H.: Elemental composition and health risk assessment of PM₁₀ and PM_{2.5} in the roadside microenvironment in Tianjin, China, *Aerosol and Air Quality Research*, 18, 1817–1827, <https://doi.org/10.4209/aaqr.2017.10.0383>, 2017.